Swiss Journal of Palaeontology (2026) 145: 1081–1110 | DOI 10.3897/sjp.145.206406

PENSOFT

Swiss Journal of Palaeontology

SGG SSP

scnat swiss academy of sciences

Research Article

Topical collection: Neogene terrestrial ecosystems (RCMNS)

Frogs and toads in the holes: Late Miocene amphibians from the Gargano Terre Rosse fissures (Southern Italy)

Andrea Villa[1], Domenico Marchitelli[2], Marco Pavia[2,3], Lorenzo Rook[4], Lars W. van den Hoek Ostende[5], Massimo Delfino[1,2]

1 *Institut Català de Paleontologia Miquel Crusafont (ICP-CERCA), Edifici ICTA-ICP, c/ Columnes s/n, Campus de la UAB, 08193 Cerdanyola del Vallès, Barcelona, Spain*

2 *Dipartimento di Scienze della Terra, Università degli Studi di Torino, Via T. Valperga Caluso 35, 10125 Torino, Italy*

3 *Research and Exhibitions, Iziko Museums of South Africa, 25 Queen Victoria Street, 8001 Cape Town, South Africa*

4 *Dipartimento di Scienze della Terra, Paleo[Fab]Lab, Università degli Studi di Firenze, via G. La Pira 4, 50121 Firenze, Italy*

5 *Naturalis Biodiversity Center, P.O. Box 9517, 2300 RA Leiden, Netherlands*

https://zoobank.org/DFFB0CB3-7491-4E7F-BDF9-AB49CF0DA168

Corresponding author: Andrea Villa (andrea.villa@icp.cat)

Academic editor: Bettina Reichenbacher ♦ **Received** 3 July 2026 ♦ **Accepted** 7 October 2026 ♦ **Published** 26 October 2026

Abstract

Nowadays, Mediterranean islands are home to several, often endemic, amphibians. Knowledge is limited, however, about amphibian palaeocommunities in the islands and palaeoislands of the Mediterranean Sea, despite the certain presence of fossils in such areas. One case with known but understudied insular amphibian fossils are the Gargano Terre Rosse, a complex of fissures in Southern Italy representing the remaining evidence of a Late Miocene (palaeo)insular fauna. More than 20 years after their first mentions, we offer here detailed descriptions of the fossil amphibians from these fissures, identifying an unbalanced and poorly diversified amphibiofauna largely dominated by *Latonia* gr. *seyfriedi* and further composed by *Hyla* gr. *arborea*, aff. *Bufotes* gr. *viridis*, and *Pelophylax* sp. Notable is the absence of urodeles, reflecting a similar trend in modern Mediterranean islands. Based on preliminary data, it seems that the Terre Rosse amphibiofauna remained generally stable along the history of the palaeoisland, potentially thanks to the resilient and adaptable ecology of the identified taxa and/or a low competition in the insular palaeoenvironment. The absence of remains from the oldest biostratigraphic phase of the Terre Rosse assemblages and the taxonomic uncertainty of the identified anurans hinder any real proposal about the dispersal or areas of origin of these frogs and toads, but their morphology, including potential character mixture, decoupling from continental evolutionary trends in the respective groups, and appearance of unusual features, support them as part of palaeocommunities already affected by evolution in insular contexts.

Keywords

Anura, Europe, insular evolution, *Latonia*, Mediterranean, Neogene

Introduction

Amphibians are well represented on Mediterranean islands (Sillero et al. 2014; Speybroeck et al. 2016, 2020; Zotos et al. 2023), often by endemic species. Most of these island amphibians are anurans, however. Only a few Mediterranean islands are inhabited by urodeles, including Corsica and Sardinia in the Western Mediterranean (Delaugerre and Cheylan 1992; Lanza et al. 2007; Di Nicola et al. 2019; Razzetti et al. 2025) and a few islands along the Greek coasts and in the Aegean Sea in the Eastern Mediterranean (Valakos et al. 2008; Tok and Çiçek 2014; Mettouris and Kornilios 2015; Cattaneo et al. 2023). This disparity might be caused by a lower

Copyright *Andrea Villa et al.* This is an open access article distributed under the terms of the Creative Commons Attribution License (CC BY 4.0), which permits unrestricted use, distribution, and reproduction in any medium, provided the original author and source are credited.

potential for overseas dispersal for urodeles (Marin da Fonte et al. 2019), possibly linked with a somewhat lower mobility (Smith and Green 2005; Cayuela et al. 2020; Reyes-Moya et al. 2022) or lower overall tolerance for saline environments (Hopkins and Brodie 2015) compared to anurans. Colonizing potential of amphibians in islands is still an open topic, but in at least some European cases it seems that urodele island populations are more likely to originate by vicariance than by dispersal (Mettouris and Kornilios 2015; Lourenço et al. 2018).

When including the fossil record in the picture, a similar distribution pattern is observed. Starting with the closure of the Tethys Ocean and the formation of the modern Mediterranean Sea in the first part of the Cenozoic (Torfstein and Steinberg 2020), several islands and palaeoislands in the Mediterranean Basin are known to have yielded amphibian fossils. On current islands, anuran fossils are known from the Late Oligocene to Holocene of the Balearic Islands (Alcover et al. 1984; Holman 1998; Sanchiz 1998; Quintana et al. 2005; Torres-Roig et al. 2017; Moncunill-Solé et al. 2026), the Miocene to Holocene of Sardinia (Kotsakis 1980; Holman 1998; Sanchiz 1998; Delfino 2002; Abbazzi et al. 2004; Venczel and Sanchíz 2006; Delfino and Rook 2008; Delfino et al. 2011), the Early Miocene of Euboea (Georgalis et al. 2019; Delfino and Georgalis 2022) and Lesbos (Vasileiadou et al. 2017), the Late Miocene and Pleistocene of Crete (Kotsakis 1982; Holman 1998; Sanchiz 1998; Georgalis et al. 2016; Delfino and Georgalis 2022), the Pleistocene to Holocene of Sicily (Holman 1998; Sanchiz 1998; Delfino 2002), the Pleistocene of Kos (Delfino and Georgalis 2022), the Middle Pleistocene of Chios (Holman 1998; Delfino and Georgalis 2022), and the Late Pleistocene to Holocene of Corsica (Vigne et al. 1997; Holman 1998) and Malta (Savona Ventura 1984; Holman 1998). On the other hand, urodele fossils only come from the Early Miocene of Lesbos (Vasileiadou et al. 2017; Delfino and Georgalis 2022) and the Early Miocene to Pleistocene of Sardinia (Delfino 2002; Abbazzi et al. 2004; Delfino et al. 2005, 2011; Venczel and Sanchíz 2006; Delfino and Rook 2008; Macaluso et al. 2021, 2022). However, it must be highlighted that the exploration of palaeoherpetofaunas in Mediterranean islands is far less advanced than the study of their current herpetofaunas, both because of implicit biases in the fossil record and of a general scarcity of studies of fossil amphibians and reptiles in these contexts.

In addition, some areas currently connected with the rest of the continental land masses surrounding the Mediterranean Sea were isolated as palaeoislands in the past (therefore fossil islands as defined by Lanza 1984), and in some cases fossil amphibians are known from when these areas were separated from the mainland. This is particularly true for the Apennine Peninsula, the modern territory of which was split into islands or archipelagos with regionalised faunas for at least part of the Neogene (Rook et al. 2006). For example, Cirilli et al. (2016) reported a few anuran fossils from Fosso della Fittaia, a Late Miocene locality in modern Tuscany, which was then part of an insular system together with the Corso-Sardinian block. Most notably, anurans are known from the highly fossiliferous karstic fissures in the Gargano Terre Rosse area, in Southern Italy. These remains were first included by Delfino (2002) in his PhD thesis, and subsequently briefly reported by Savorelli et al. (2025) in their recent overview of the Terre Rosse. However, they were never the subject of a dedicated and detailed publication. Previous reports mentioned the presence of discoglossids, hylids, bufonids, and ranids (Delfino 2002; Savorelli et al. 2025).

With this paper, we aim at filling this long-lasting gap, by: 1) describing and identifying amphibian remains from the Gargano Terre Rosse; 2) highlighting and discussing distribution and abundance patterns in the context of the different fissures and stratigraphic hypotheses on the evolutionary phases of the Gargano insular fauna; and 3) conducting a preliminary investigation into the phylogenetic relationships of the most abundant amphibian in the sample.

Geological and palaeontological setting

In the geopalaeontological literature, the name Gargano Terre Rosse refers to a series of red soil deposits in palaeokarstic fissures developed in Mesozoic limestone, located in the Apulia region of southern Italy. The palaeokarstic network extends primarily on the northwestern slopes of the Gargano promontory, between the towns of Apricena and Poggio Imperiale, and yielded a very large number of fossils of vertebrates, whose scientific relevance started to be explored by Dutch researchers led by Matthijs Freudenthal in the late 60s/early 70s of the 20th century (Freudenthal 1971; Masini et al. 2010). The history and scientific results of research on the Gargano Terre Rosse deposits were summarized by Masini et al. (2010) and, more recently, by Savorelli et al. (2025), to which the reader is referred for more details. Here, it is important to mention that the vertebrates recovered from the fissures testify for the occurrence of a peculiar fauna, likely evolving in insular conditions and composed of endemic taxa. These assemblages are sometimes referred to as the "*Mikrotia* fauna" (e.g. Freudenthal et al. 2013), after the most common representative taxon in them, the giant endemic murid *Mikrotia* Freudenthal, 2006. Amphibians and reptiles from the Terre Rosse fissures include anurans, crocodylians, turtles, and squamates (Delfino 2002; Masini et al. 2010; Savorelli et al. 2025). Crocodylian remains are rare but represented the first robust evidence of the dispersal of the extant genus *Crocodylus* Laurenti, 1768 in Europe (Delfino et al. 2007). Chelonian remains were recently tentatively referred to as the oldest record of *Solitudo* Valenti et al., 2022, a genus of Mediterranean insular giant tortoises (Georgalis et al. 2025). Squamates are still the ongoing subject of a thorough study under modern osteological and palaeontological knowledge of these reptiles in Europe, but Villa and Delfino (2019) stated that the gecko fossils might represent a new taxon.

The chronology of the Gargano Terre Rosse fissure fillings is still subject to debate. The most recent overview by Savorelli et al. (2025) indicated a Late Miocene age for the faunal complex overall, but uncertainty still surrounds the actual lower age limit. Masini et al. (2010, 2013) and Savorelli et al. (2016, 2025) proposed a biostratigraphic framework for some of the fissures, based on mammal assemblages and comprised of five phases (from phase 0 to 4, some with subphases). Only some of the fissures with amphibian fossils can currently be attributed to a specific phase, whereas most of them are referred to an indeterminate phase for the time being, pending a biostratigraphic study of the relevant small mammals. From older to younger, fissures discussed in this paper are distributed as follows:

- Phase 1a: Rinascita 1.
- Phase 1b: Biancone 1, F15, and F21B.
- Phase 2a: Cantatore 3A and Fina D.
- Phase 2c: F1.
- Phase 3a: F9 and F9 S1 UD.
- Phase 3b: Chirò 20A, Chirò 20C, and Chirò 24.
- Phase 3c: San Giovannino.
- Phase 4: F32 G.A., F32/1, F32/2, F32/3, F32/4, F32/7, F32/8, F32/9, F32/10, and F32/11.

Phase assignment is currently missing for the following fissures: Biancone 2, Bosco 2, Bosco 3, Bosco 4, Chirò, Chirò 2N, Chirò 3, Chirò 7A, Chirò 8, Chirò 9, Chirò 12, Chirò 14, Chirò 15, Chirò 22, Chirò 26, Chirò 28, Chirò 80/1 NL, F15 err, F23, Falcone 2A, Fina 2013, Fina H, Fina L, Gervasio 5, I Tre Fossi 21a, Lesina - Bivio S. Nazario, Nazario, Pirro 77/2, Pirro 80/1, Pizzicoli, Pizzicoli 1/2007, Pizzicoli 2/2003, Pizzicoli 11, Pizzicoli II, Pizzicoli IV, San Giovannino F2 parte bassa, San Nazario - bivio Lesina sinistra, Tre Fossi, and Tre Fossi 2A. However, a chronological order for most of these assemblages was suggested by Freudenthal (1976) based on the stage in evolution of *Mikrotia*.

Material and methods

The herein studied material includes all the recognized amphibian fossils recovered from the Late Miocene fissure fillings of the Gargano Terre Rosse. The fossils belong to three different collections, hosted in the Università degli Studi di Firenze in Florence, Italy, the Università degli Studi di Torino in Turin, Italy, and Naturalis Biodiversity Center in Leiden, The Netherlands. The anatomical terminology follows mainly Sanchiz (1998), complemented by terms from Gómez and Turazzini (2016) and Sorbelli et al. (2025). Pictures of selected fossils were taken with a Leica M205 microscope equipped with LAS (Leica Application Suite) v. 4.13 and with a Canon EOS 5D Mark II camera equipped with a 100 mm macro lens. To reduce manuscript length, a complete list of the studied material, with collection numbers, is provided in Suppl. material 1. We calculated the minimum number of individuals (MNI) per fissure and as a whole. Raw results for this calculation are also provided in Suppl. material 1. Distribution of MNI and number of identifiable specimens (NISP) per taxon and fissures were calculated and plotted using Past v. 5.3 (Hammer et al. 2001). Occurrences with indeterminate fissure provenance were used to calculate the total NISP and MNI, but not to compute distributions per fissure.

We analyzed the phylogenetic relationships of the painted frog, *Latonia* von Meyer, 1843, from Gargano using a maximum parsimony approach in TNT v. 1.6 (Goloboff and Morales 2023). We added a new operational taxonomic unit (OTU) based on the Gargano occurrence with Mesquite v. 4.02 (Maddison and Maddison 2025) to the matrix published by Sorbelli et al. (2025). We performed the analysis following the same settings and protocol as the latter authors, replicating both their second and third iterations, that is, deactivating all OTUs with less than 50% of scored characters and then also *Eodiscoglossus* Villalta, 1954 and *Wealdenbatrachus* Fey, 1988. Trees were visualized using FigTree v. 1.4.4 (http://tree.bio.ed.ac.uk/software/figtree/). The matrix is available as a Nexus file in the Suppl. material 2.

Institutional abbreviations. **DSTF-GH**, Gargano palaeoherpetological collection, Dipartimento di Scienze della Terra, Università degli Studi di Firenze, Florence, Italy; **MGPT-PU**, Museo di Geologia e Paleontologia Collections, Dipartimento di Scienze della Terra, Università degli Studi di Torino, Turin, Italy; **MGPT-MDHC**, Massimo Delfino Herpetological Collection, Dipartimento di Scienze della Terra, Università degli Studi di Torino, Turin, Italy; **RGM**, Naturalis Biodiversity Center, Leiden, The Netherlands.

Systematic Palaeontology

Class Amphibia Linnaeus, 1758
Order Anura Duméril, 1805
Family Discoglossidae Günther, 1858
Genus *Latonia* von Meyer, 1843
***Latonia seyfriedi* von Meyer, 1843**

Latonia* gr. *seyfriedi
Figs 1–4

Material. *Biancone 1*: one atlas, five trunk vertebrae, and two sacral vertebrae. ***Bosco 2*:** one angular, one atlas, eight trunk vertebrae, one sacral vertebra, one urostyle, two scapulae, and two ischia. ***Bosco 4*:** three trunk vertebrae, three ribs, and one radioulna. ***Cantatore 3A*:** one prootic-exoccipital, one trunk vertebra, one sacral vertebra, and one rib. ***Chirò*:** three maxillae. ***Chirò 2N*:** one urostyle. ***Chirò 3*:** five maxillae, two frontoparietals, two angulars, three atlases, nine trunk vertebrae, one sacral vertebra, one coracoid, one scapula, three humeri, three ilia, and one femur. ***Chirò 7A*:** one angular, one trunk vertebra, and one sacral vertebra. ***Chirò 8*:** one

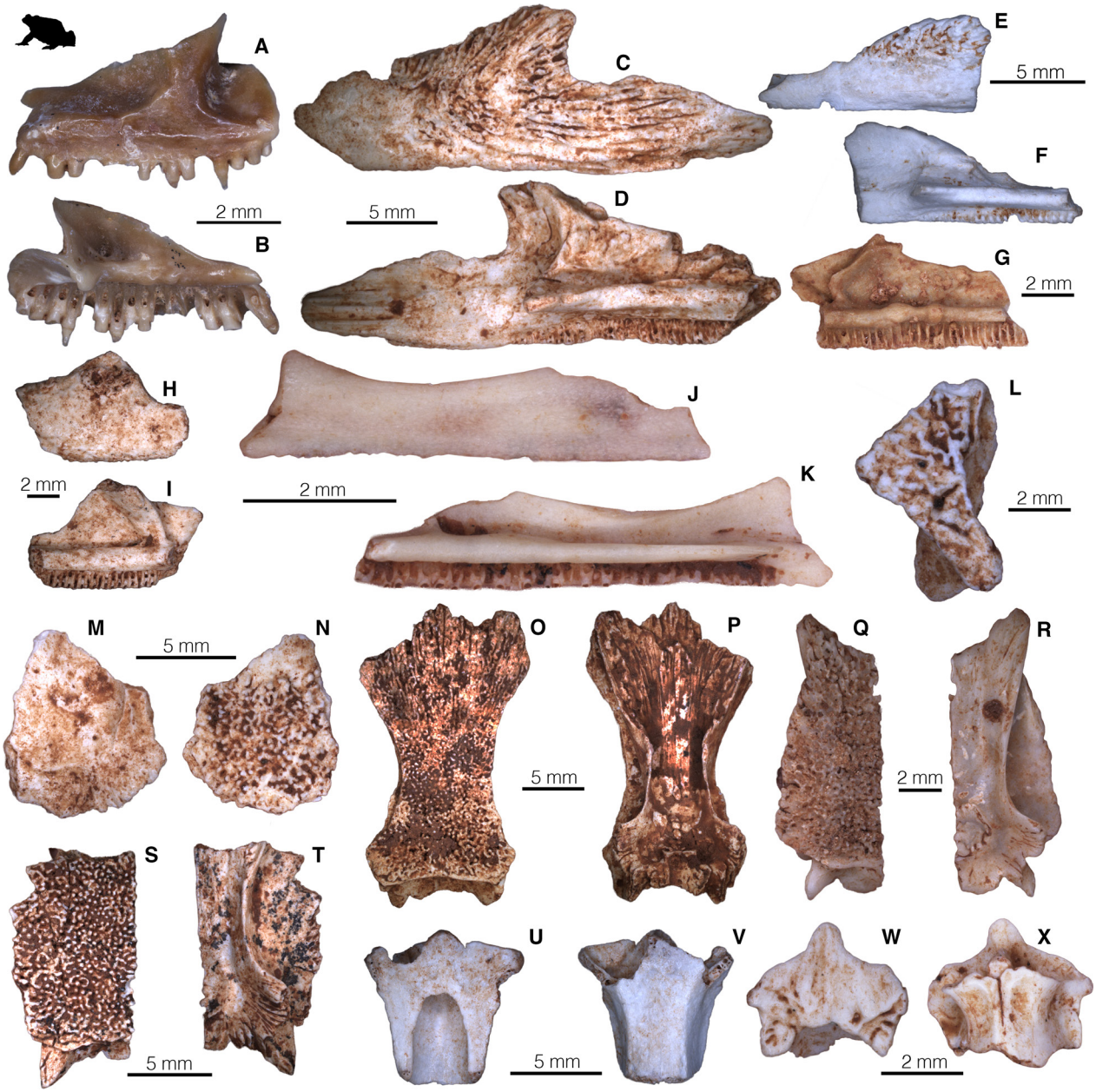


Figure 1. *Latonia* gr. *seyfriedi* from the Late Miocene of the Gargano Terre Rosse. **A, B.** Right premaxilla (DSTF-GH 213) in anterior (**A**) and posterior (**B**) views; **C, D.** Left maxilla (MGPT-PU 142571) in lateral (**C**) and medial (**D**) views; **E, F.** Left maxilla (MGPT-PU 138955) in lateral (**E**) and medial (**F**) views; **G.** Left maxilla (DSTF-GH 417) in medial view; **H, I.** Right maxilla (DSTF-GH 115) in lateral (**H**) and medial (**I**) views; **J, K.** Right maxilla (DSTF-GH 308) in lateral (**J**) and medial (**K**) views; **L.** Left squamosal (RGM 452677) in lateral view; **M, N.** Left nasal (RGM 451938) in ventral (**M**) and dorsal (**N**) views; **O, P.** Frontoparietal (MGPT-PU 142654) in dorsal (**O**) and ventral (**P**) views; **Q, R.** Frontoparietal (MGPT-PU 139988) in dorsal (**Q**) and ventral (**R**) views; **S, T.** Frontoparietal (RGM 455134) in dorsal (**S**) and ventral (**T**) views; **U, V.** Sphenethmoid (MGPT-PU 138927) in dorsal (**U**) and ventral (**V**) views; **W, X.** Sphenethmoid (MGPT-PU 138906) in dorsal (**W**) and ventral (**X**) views.

atlas and one trunk vertebra. ***Chirò 9*****:** three frontoparietals, one prootic-exoccipital, one angular, and one trunk vertebra. ***Chirò 12*****:** five prootic-exoccipitals, eight trunk vertebrae, one sacral vertebra, and 11 humeri. ***Chirò 15*****:** one tibiofibula. ***Chirò 20A*****:** one humerus, one tibiofibula, and one tibiale. ***Chirò 20C*****:** one coracoid. ***Chirò 22*****:** one humerus. ***Chirò 24*****:** one maxilla, one nasal, one frontoparietal, one angular, two atlases, seven trunk vertebrae, three sacral vertebrae, three urostyles, and six humeri. ***Chirò 26*****:** one femur. ***Chirò 28*****:** three squamosals, one atlas, five trunk vertebrae, two sacral vertebrae, one scapula, three humeri, and one ilium. ***Chirò 80/1 NL*****:** one maxilla. ***F1*****:** one maxilla and one angular. ***F9*****:** two maxillae, two trunk vertebrae, and one tibiofibula. ***F9 S1 UD*****:** one trunk vertebra and one urostyle. ***F15*****:** one atlas, two trunk vertebrae, and one sacral vertebra. ***F15 err.*****:** one trunk vertebra, one ilium, and one tibiale. ***F21b*****:** one maxilla and one urostyle. ***F23*****:** one sacral



Figure 2. *Latonia* gr. *seyfriedi* from the Late Miocene of the Gargano Terre Rosse. **A–F.** Right prootic-exoccipital (MGPT-PU 138929) in anterior (**A**), posterior (**B**), dorsal (**C**), ventral (**D**), lateral (**E**) and medial (**F**) views; **G.** Right prootic-exoccipital (RGM 453448) in posterior view; **H, I.** Left prootic-exoccipital (RGM 452328) in posterior (**H**) and dorsal (**I**) views; **J–M.** Right prootic-exoccipital (RGM 451484) in anterior (**J**), posterior (**K**), dorsal (**L**) and ventral (**M**) views; **N–Q.** Right angular (RGM 452074) in dorsal (**N**), lateral (**O**), ventral (**P**) and medial (**Q**) views.

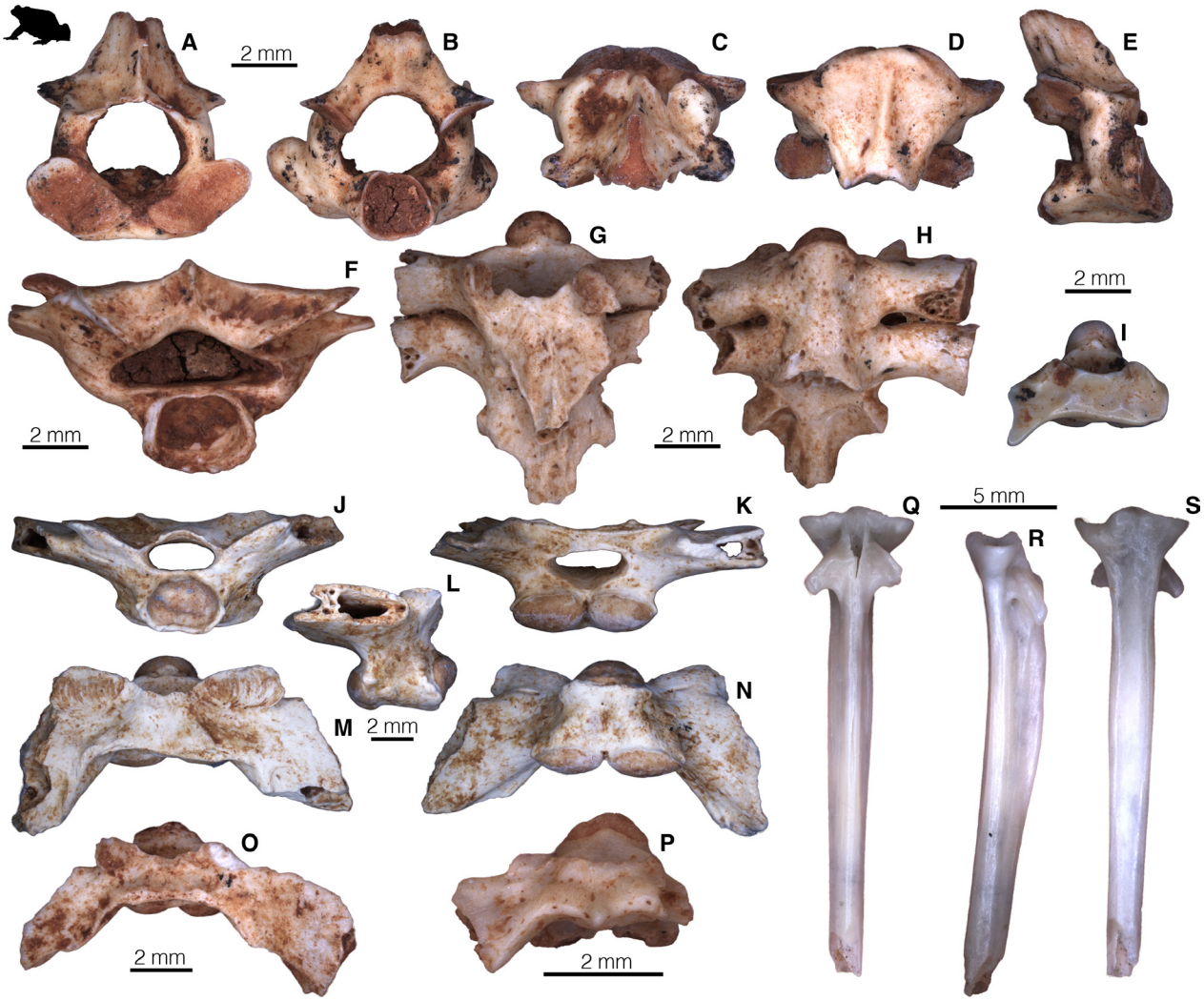


Figure 3. *Latonia* gr. *seyfriedi* from the Late Miocene of the Gargano Terre Rosse. **A–E.** Atlas (DSTF-GH 127) in anterior (**A**), posterior (**B**), dorsal (**C**), ventral (**D**) and right lateral (**E**) views; **F.** Trunk vertebra (RGM 452051) in posterior view; **G, H.** Fused trunk vertebrae (RGM 452052) in dorsal (**G**) and ventral (**H**) views; **I.** Sacral vertebra (MGPT-PU 150975) in dorsal view; **J–N.** Sacral vertebra (DSTF-GH 209) in anterior (**J**), posterior (**K**), right lateral (**L**), dorsal (**M**) and ventral (**N**) views; **O.** Sacral vertebra (RGM 452056) in dorsal view; **P.** Sacral vertebra (DSTF-GH 335) in dorsal view; **Q–S.** Urostyle (MGPT-PU 138930) in dorsal (**Q**), left lateral (**R**) and ventral (**S**) views.

vertebra, one ilium, and one tibiofibula. ***F32 G.A.*:** one trunk vertebra. ***F32/1*:** one maxilla. ***F32/2*:** one trunk vertebra. ***F32/3*:** one trunk vertebra and one urostyle. ***F32/4*:** one trunk vertebra and one sacral vertebra. ***F32/7*:** one trunk vertebra. ***F32/8*:** one premaxilla and one trunk vertebra. ***F32/9*:** one humerus. ***Falcone 2A*:** one trunk vertebra and three ribs. ***Fina 2013*:** two frontoparietals. ***Fina D*:** one atlas, one urostyle, one humerus, and one ilium. ***Fina H*:** one trunk vertebra and one radioulna. ***Fina L*:** one trunk vertebra. ***I Tre Fossi 21a*:** two trunk vertebrae and two humeri. ***Lesina, Bivio S. Nazario*:** one trunk vertebra. ***Nazario*:** one clavicle and one radioulna. ***Pirro 77/2*:** two trunk vertebrae. ***Pirro 80/1*:** one premaxilla and one maxilla. ***Pizzicoli*:** two maxillae and three trunk vertebrae. ***Pizzicoli 2/2003*:** one ilium. ***Pizzicoli II*:** two maxillae, one sphenethmoid, one prootic-exoccipital, one angular, two trunk vertebrae, one urostyle, five humeri, three radioulnae, and three tibiofibulae. ***Pizzicoli IV*:** five maxillae, four fragments of frontoparietal, one sphenethmoid, one angular, four trunk vertebrae, one sacral vertebra, one scapula, two ilia, and two tibiofibulae. ***Rinascita 1*:** one maxilla, seven trunk vertebrae, one urostyle, and five humeri. ***San Giovannino*:** one maxilla, six frontoparietals, two prootic-exoccipitals, one trunk vertebra, one urostyle, two humeri, two ilia, two ischia, two femurs, and two tibiale. ***San Giovannino F2 parte bassa*:** one maxilla, one prootic-exoccipital, one angular, one atlas, five trunk vertebrae, three urostyles, one coracoid, two radioulnae, four tibiofibulae, and two tibiale. ***San Nazario – bivio Lesina sinistra*:** one maxilla and one femur. ***Tre Fossi*:** one maxilla and two frontoparietals. ***Tre Fossi 2A*:** one prootic-exoccipital and one trunk vertebra. ***"Terre Rosse", locality indet.*:** two maxillae, one angular, and one ilium.

Descriptions. ***Premaxillae*** (Fig. 1A, B). The premaxilla DSTF-GH 213 (Fig. 1A, B) is large and well preserved, even though it misses most of the pars facialis. The bone is mediolaterally elongated, with a well-developed and



Figure 4. *Latonia* gr. *seyfriedi* from the Late Miocene of the Gargano Terre Rosse. **A.** Right clavicle (RGM 454924) in dorsal view; **B.** Right coracoid (RGM 452108) in dorsal view; **C, D.** Right scapula (MGPT-PU 142612) in dorsal (**C**) and ventral (**D**) views; **E–G.** Left humerus (RGM 451650) in dorsal (**E**), medial (**F**) and ventral (**G**) views; **H, I.** Right radioulna (MGPT-PU 138925) in lateral (**H**) and medial (**I**) views; **J, K.** Right ilium (RGM 451211) in lateral (**J**) and medial (**K**) views; **L.** Ischium (RGM 455245) in left lateral view; **M.** Left femur (RGM 452460) in ventral view; **N, O.** Right tibiofibula (MGPT-PU 138931) in ventral (**N**) and dorsal (**O**) views; **P, Q.** Left tibiofibula (MGPT-PU 139996) in dorsal (**P**) and ventral (**Q**) views; **R, S.** Left tibiale (RGM 1286490) in anterior (**R**) and posterior (**S**) views.

rounded pars palatina on the medial end. Lateral to this, the lamina horizontalis is short and rounded. The crista dentalis covers the complete mediolateral width of the premaxilla (Fig. 1B). Teeth are pleurodont, pedicellate, closely packed, cylindrical and narrow; the preservation allows for a complete count of the tooth position, resulting

in a number of 16. In dorsal view, a wide cavity with a foramen in the middle is visible posterior to the base of the laminar pars facialis. The anterior surface is smooth (Fig. 1A). DSTF-GH 284 is a slightly smaller premaxilla, missing the pars facialis. The overall morphology is similar, but this specimen hosts 13 tooth positions.

Maxillae (Fig. 1C–K). MGPT-PU 142571 (Fig. 1C, D) is a very large maxilla, preserving roughly the posterior half of the bone. Medially, the bone hosts a thick and short lamina horizontalis (Fig. 1D), with a convex medial surface. Posteriorly, the lamina ends with a long and thick processus pterygoideus, with the tip broken. Dorsally, the lamina is shallowly grooved. Ventral to the lamina, the tooth row ends very slightly posterior to the processus pterygoideus. The tooth positions are closely packed. None of the teeth are preserved, with only small fragments of cylindrical pleurodont teeth remaining. The posterior end of the bone bears a long and pointed processus posterior. Dorsally, the processus zygomaticomaxillaris is present; it is broken, so its complete development cannot be assessed. The margo orbitalis is shallowly concave. Ventral to the processus zygomaticomaxillaris, a clear posterior depression is visible, defined anteriorly by a marked curved ridge. The lateral surface of this maxilla displays a well-developed sculpturing made up of small tubercles and ridges (Fig. 1C). The sculpturing covers most of the preserved portion of the bone, except for the anteriomost preserved end. This absence can be potentially interpreted as secondary loss, because the surface of the bone is slightly rough and the preserved sculpturing is not completely coossified with the underlying bone.

MGPT-PU 138955 (Fig. 1E, F) and 142626 and RGM 452065, 452067 and 453464 represent more or less the same portion of bone, but they are much smaller. MGPT-PU 138904, 139995 and 142681, as well as DSTF-GH 340 are also smaller, but they also preserve a more anterior portion of the bone, reaching up or almost up to the processus palatinus. The morphology of the preserved portions is almost the same as for MGPT-PU 142571, but the posterior depression is much shallower and not marked anteriorly by a ridge (Fig. 1F). Moreover, on the lateral surface, the dermal sculpturing is much less developed and mostly arranged around the processus zygomaticomaxillaris (Fig. 1E). The rest of the surface is highly irregular. MGPT-PU 142681 preserves the complete processus pterygoideus, which is long and pointed. Notably, the posterior end of the tooth row is at the same level as the processus pterygoideus in MGPT-PU 138955 (Fig. 1F) and DSTF-GH 340. The small fragment RGM 455140 only preserves the area with the processus pterygoideus. In this specimen as well, the tooth row ends level with the process. Laterally, in spite of the limited fragmentary nature of the specimen, remnants of the dermal sculpturing are present.

DSTF-GH 308 (Fig. 1J, K) is a very small and gracile maxilla. It is moderately well preserved, missing only the most anterior portion and the posteriormost end. Most of the morphology is comparable to the larger specimens, with a short and rounded lamina horizontalis, a long processus pterygoideus, a shallowly concave margo orbitalis, and the presence of a processus zygomaticomaxillaris. There is no posterior depression (Fig. 1K). The preserved tooth row counts 36 tooth positions (but, as said, the anteriormost portion is missing) and ends posterior to the end of the lamina horizontalis. Part of the gutter-like processus facialis is preserved. The lateral surface is completely smooth (Fig. 1J), even devoid of rugosities. DSTF-GH 133 is similar, but slightly less preserved.

The other maxillae assigned to this taxon are variably, but less-preserved fragments, medium to large or even very large in size. They all represent more anterior portions of the bone with respect to previous specimens. Except for DSTF-GH 115 (Fig. 1H, I), they have a smooth lateral surface. A certain roughness is visible in some of these specimens, so it is not clear whether the smooth morphology is true or, maybe most likely, originates from a loss of the dermal sculpturing. At least DSTF-GH 115, which is the fragment of a large maxilla, shows some remnants of the dermal sculpturing (Fig. 1H). This same fragment and DSTF-GH 417 (Fig. 1G) preserve the processus facialis and the surrounding area. The process is laminar, anterodorsally inclined and gutter-shaped. DSTF-GH 417 also presents two distinct pathologic bulges on the lamina horizontalis (Fig. 1G).

Squamosals (Fig. 1L). All three squamosals are very fragmentary, but they appear moderately large and robust. The lamella alaris clearly hosted a dense and well-developed dermal sculpturing (Fig. 1L). The latter is made up of small tubercles, which in some cases fuse to originate short ridges.

Nasal (Fig. 1M, N). The only fragmentary nasal, RGM 451933 (Fig. 1M, N), only preserves part of the posteromedial corner of the bone. Both the posteromedial extension for the contact with the frontoparietal and the processus paraorbitalis are broken off. The fossil is very large and robust. Ventrally (Fig. 1M), a low ridge marks the lateral and posterior portions of the surface, where the nasal overlaps the sphenethmoid. The dorsal surface is almost completely covered by a moderately dense sculpturing (Fig. 1L). Only the most anterior preserved portion of the fragment appears smooth. The sculpturing is composed of small tubercles, only rarely fusing up into very short ridges.

Frontoparietals (Fig. 1O–T). MGPT-PU 142654 (Fig. 1O, P) is the largest and best preserved frontoparietal. It is very large, unpaired and robust, with no visible suture at midline in ventral view (Fig. 1P). The ventral surface is strongly concave, due to a distinct development of the pars contacta on the sides. In ventral view, each pars contacta has a sigmoid course, and the anterior portion gradually lowers. By the posterior end of each pars contacta, a thick margo prooticum is visible, for a robust articulation with the prootic bone. The incrassatio frontoparietalis is clearly divided into two portions (Fig. 1P): the elongated and rather narrow anterior one and the subtrapezoidal posterior one, bordered by a raised rim (which is, however, mostly broken off). The two portions of the incrassatio are separated by a wide gap, and a marked step is present at

the anterior margin of the posterior portion. In the anterior half of the bone, an evident striation is visible, diverging towards the anterolateral corners (Fig. 1P). Dorsally, the frontoparietal is almost completely covered by a dense dermal sculpturing (Fig. 1O), composed of strongly packed and small tubercles, which sometimes merge into short vermicular structures. By the anterior end of the bone, the tubercles are united into linear structures directed more or less longitudinally. The sculpturing is closely appressed to the underlying bone, but, as clearly visible at least by the left anterolateral corner (which is the only area of the sculptured surface with a clear breakage), empty spaces are present between them, indicating a secondary ossification of the sculpturing. In dorsal view, the bone has an hourglass shape, with strongly concave lateral margins (Fig. 1O). This seems not to be the original shape of the bone: even though there is no clear sign of breakage laterally, a certain degree of asymmetry in the development of the tectum supraorbitale (Fig. 1P) hints towards the loss of part of the facies dorsalis. Nevertheless, the facies dorsalis seems to develop at least to some degree in lateral direction to cover the orbits: as said, a narrow portion of tectum supraorbitale is still visible in ventral view, more preserved on the right (Fig. 1P). The preserved right anterolateral corner clearly shows a short horn. The posterior end of the frontoparietal displays a small sloping surface, which is the only unsculptured part and ends posteriorly with the margo occipitalis (Fig. 1O). The margin itself is broken, preventing the evaluation of the potential presence of a processus posterior, but it was likely convex. A very low and rounded longitudinal ridge is present at the midline of the sloping surface. Each posterolateral corner bears a short and wide processus paraoccipitalis, which extends in posterior direction and surpasses the margo occipitalis for about half of its length.

MGPT-PU 139988 (Fig. 1Q, R) and RGM 455134 (Fig. 1S, T) are frontoparietals much smaller than the previous one. They are unpaired and preserve only the left half of the bone. RGM 455134 further misses the anterior left corner. The overall morphology recalls that of MGPT-PU 142654, but with some differences. The ventral surface hosts a two-portioned incrassatio frontoparietalis (Fig. 1R, T), with the same shape as in MGPT-PU 142654 (Fig. 1P). However, the rim of the posterior portion is low, and there is no step at its anterior margin. There is no striation on the anterior half of the ventral surface of these bones. The pars contacta is straight, not sigmoid, with an anterolateral to posteromedial course. The margo prooticum (Fig. 1R, T) is less thick than in MGPT-PU 142654 (Fig. 1P), but still proportionally robust. In dorsal view, the facies dorsalis is completely covered by a well-developed dermal sculpturing (Fig. 1Q, S), as in MGPT-PU 142654 (Fig. 1O), but this is slightly less dense in MGPT-PU 139988 (Fig. 1Q). Moreover, in both MGPT-PU 139988 (Fig. 1R) and RGM 455134 (Fig. 1T), the tectum supraorbitale is clearly strongly developed, with a roughly straight lateral margin. Anteriorly, the left anterolateral horn is preserved in MGPT-PU 139988 (Fig. 1Q, R). At the posterior end of the bone, the smooth sloping surface is less inclined than in MGPT-PU 142654 (Fig. 1O). The margo occipitalis is convex. Due to the preservation, it is not possible to evaluate the presence or absence of a longitudinal ridge. The left processus paraoccipitalis is short, pointed and directed posterolaterally; it extends beyond the margo occipitalis for half of its length.

Other fragments of frontoparietals are present in the sample. These are just portions of the bones, covered with the same sculpturing as the largest specimen. Portions of the pars contacta and of a well-developed tectum supraorbitale are also visible in some of the specimens.

Sphenethmoids (Fig. 1U–X). The largest sphenethmoid, MGPT-PU 138927 (Fig. 1U, V), is almost complete, longer than wide, strongly dorsoventrally compressed and distinctly enlarging at the anterior end. The laminae supraorbitalis seem poorly developed, but these might be impacted by damage. In dorsal view (Fig. 1U), a deep and moderately narrow U-shaped notch exposes the inner antrum pro lobo olfactorio. The dorsal surface of the bone is flat and very slightly striated. The ventral surface (Fig. 1V) hosts a wide articular surface for the parasphenoid, which is also slightly striated and widens anteriorly. The trabeculae are completely missing. At the anterior end of the sphenethmoid, the two antri olfactorii are separated by a narrow septum nasi, which projects shallowly anteriorly (originating a short and rounded point in dorsal view). In each antrum, a very wide foramen nervo I is present closely appressed to the septum, whereas a small foramen nutritium is located at the lateral margin.

MGPT-PU 138906 (Fig. 1W, X) is a much smaller specimen, slightly damaged at the anterior and posterior margins. The bone is wider than long (but part of the posterior portion is likely missing) and dorsoventrally compressed. On the dorsal surface (Fig. 1W), an anteroposterior striation is visible. Anteriorly, the septum nasi projects in a distinct point. The antrum pro lobo olfactorio is visible through a shallow notch. Along the sides, the laminae supraorbitalis are moderately developed. Ventrally, a suture line is visible (Fig. 1X), crossing longitudinally the bone at midline. The ventral surface does not show striae. The trabeculae are mostly missing, but judging from the right side, they were individualized from the main body of the bone. In anterior view, the foramina nervo I are very wide, standing out in each antrum olfactorium. The related foramen nutritium is very small and located at the lateral margin of the antrum.

Prootic-exoccipitals (Fig. 2A–M). Prootic-exoccipitals are stocky and go from medium to large in size. The preservation goes from good to varying degrees of damage. MGPT-PU 138929 (Fig. 2A–F) is the largest and one of the best-preserved specimens. The prootic-exoccipitals are composed by a main median body, including the exoccipital portion and articulating medially with the contralateral element, and the prootic portion extending laterally. In dorsal view (Fig. 2C, I, L), the area for the articulation with the frontoparietal is marked and slightly striated. The crista parotica extends laterally as a long

process with a forked distal end. The posterior branch (processus prooticus caudalis *sensu* Sorbelli et al. 2025) of this forked end is twice as long as the anterior branch (processus prooticus rostralis brevis *sensu* Sorbelli et al. 2025). On the posterior margin of the prootic-exoccipital, the prominentia ducti semicircularis posterioris is present. It is often broken off, but complete prominentiae are also present in some specimens (Fig. 2I, L). This structure is short, not extending posterior to the condyle in dorsal view. It has a wide basis in all specimens. In most cases where it is complete (e.g. RGM 451484; Fig. 2J–M), it narrows posteriorly to originate a triangular shape. However, only in RGM 452328 (Fig. 2H, I), it remains wide for its entire length. Ventral to the crista parotica, there is a robust structure for the contact with the palatoquadrate. In anterior view (Fig. 2A, J), this structure and the crista are separated by the narrow sulcus venae jugularis. In the middle of the anterior surface, the orifice for the sixth cranial nerve stands out: this is a wide cavity into which two smaller foramina open. In lateral view, there is a very wide fenestra ovalis (Fig. 2E). In medial view, the inner surface of the cranial cavity is visible, with several foramina. A wide and anteroposteriorly elongated cavity in the middle of this inner surface, where several smaller foramina open, likely represents the fusion of the acoustic foramina (Lemierre and Blackburn 2022). Dorsal to this, the small endolymphatic foramen is present, whereas posterior is the large foramen jugulare, where also smaller foramina converge. The foramen jugulare further opens posterolaterally and is distinctly visible in ventral view (Fig. 2D, M). The ventral surface (Fig. 2D, M) of the prootic-exoccipital is rough. On the posterior side of the bone (Fig. 2B, G, H, K), the most significant structure is the teardrop-shaped condylus occipitalis. At the ventrolateral side, a small bony outgrowth is present in MGPT-PU 138929 (Fig. 2B), but not in the other specimens (Fig. 2G, H, K). Between the prominentia ducti semicircularis posterioris and the condylus occipitalis, a low vertical ridge is present in most specimens except DSTF-GH 141, RGM 451488, 453448 (Fig. 2G) and 455197. The ridge is sigmoid in MGPT-PU 138929 (Fig. 2B), RGM 451487, 452328 (Fig. 2H) and 455301 and straight in RGM 451484 (Fig. 2K), 451485 and 451486. It is connected to the prominentia but separated from the condyle by a gap, which is short when the crista is sigmoid and larger when it is straight.

Angulars (Fig. 2N–Q). Angulars are large, with a gentle curve at the anterior end. Some specimens, like e.g. the almost-complete DSTF-GH 74, are very large. The robustness of these fossils increases with size. Two processes are present on the medial side of the posterior portion (Fig. 2N, Q): a low and wide processus paracoronoideus, followed by a narrower processus coronoideus. The latter is directed medially and not extended posteriorly. In medial view (Fig. 2Q), the dorsal surface of the processus paracoronoideus is straight (dorsally concave only in DSTF-GH 74 and 128, and RGM 451286), and the processus coronoideus clearly projects in dorsal direction. At the same level, a shallow concavity is visible on the lateral surface, marked ventrally by a sharp crista mandibulae externa (Fig. 2O). Only in DSTF-GH 74 is the extremitas spatulata completely preserved: it is wide and proportionally short.

Atlases (Fig. 3A–E). The atlases are either small (e.g. DSTF-GH 337) or very large (e.g. DSTF-GH 127; Fig. 3A–E), with dorsolaterally inclined anterior cotyles (defining an angle of roughly 90°; Fig. 3A) and a subcircular posterior cotyle (Fig. 3B). The anterior cotyles are closely spaced, but they do not merge medially. The neural canal is wide and circular in anterior view. The ventral surface of the centrum hosts a low longitudinal ridge (Fig. 3D). The roof of the neural arch is rather long; dorsally, it hosts a very low carina neuralis and a wide and truncated posterior point (Fig. 3C). The postzygapophyses are well projected posterolaterally.

Trunk vertebrae (Fig. 3F–H). Different size classes are represented within the sample of available trunk vertebrae, from small to medium to large fossils. The vertebrae are preserved in different conditions, spanning from almost complete specimens to more fragmentary ones. RGM 452052 (Fig. 3G, H) is represented by two vertebrae fused together. All the trunk vertebrae are opisthocoelous, with a cylindrical or subcylindrical, slightly dorsoventrally compressed, centrum. The neural canal is subtrapezoidal and strongly dorsoventrally compressed (Fig. 3F). The neural arch is robust and long (Fig. 3G), without or with a very low carina neuralis, but with a well-developed posterior point, which can be either short and rounded or longer and more pointed. The zygapophyses are wide and subelliptical. The transverse processes are wide and either laminar or cylindrical; they are located below the prezygapophyses. RGM 452051 presents a swelling of the posterior margin of the neural arch wall, of potential pathological origin (Fig. 3F).

Ribs. The isolated ribs are slender and straight, with slightly widened distal ends. All of them bear a short and pointed uncinate process on the dorsal surface.

Sacral vertebrae (Fig. 3I–P). The sacral vertebra DSTF-GH 209 (Fig. 3J–N) is well preserved, very large and robust. The most distal parts of the transverse processes are broken off. Ventrally, the centrum is short and subtrapezoidal (Fig. 3N), with one anterior and two posterior condyles. All condyles are subelliptical. The two posterior ones are closely appressed (Fig. 3K). In anterior view, the neural canal is subpentagonal and dorsoventrally compressed (Fig. 3J). The dorsal surface of the neural arch bears no carina neuralis and no ridges (Fig. 3M). The transverse processes are clearly expanded to a moderate degree in posterolateral direction; however, the breakage does not allow to recognize the complete expansion, nor to describe the inclination of their anterior margin. The prezygapophyses are wide and subelliptical, with the main axis roughly aligned mediolaterally. Other specimens share the same morphology, but they are smaller or much smaller, although, e.g., RGM 452658 and 452659 are still rather large.

Inclination of the transverse processes can be evaluated in some of these: they clearly have a posterolaterally inclined anterior margin in MGPT-PU 150975 (Fig. 3I), DSTF-GH 344, RGM 452056 (Fig. 3O) and 453236, and a straight one in DSTF-GH 335 (Fig. 3P), RGM 451285, 451919, 452658, 452659 and 454617. RGM 451285, 452056 (Fig. 3O), 452658, and 452659 further preserve either one or both almost complete transverse processes, showing that the distal expansion of the fan-shaped process is gradual and overall moderate.

Urostyles (Fig. 3Q–S). The size of the urostyles varies from large (especially MGPT-PU 138930; Fig. 3Q–S) to medium or even small-sized. They are straight bones, expanding at the anterior end, where the fossae condyloideae are located. In anterior view, the fossae are suboval or subtriangular (with the apex directed laterally), dorsoventrally compressed and closely appressed medially. The canalis coccygeus is small and subcircular. Anteriorly, two small transverse processes are present, directed posterolaterally and with truncated distal end (Fig. 3Q). Dorsally, the urostyle shows no crista dorsalis. A dorsal longitudinal opening is present in all cases, but its extension varies: it runs, e.g., for the entire urostyle in DSTF-GH 110, but it is limited only to a shallow aperture at about mid-length in MGPT-PU 138930 (Fig. 3Q) and to the posterior end in DSTF-GH 185. On the lateral sides of the urostyle, one foramen is present posteroventral to each transverse process (Fig. 3R). Short and asymmetrical lateral laminae are present only in a few specimens (e.g. DSTF-GH 185).

Clavicle (Fig. 4A). RGM 454924 (Fig. 4A) is a very small, slender and strongly curved clavicle fragment. Mainly the lateral end is preserved, showing the expanded area lodging the articulation with the pars acromialis of the scapula.

Coracoids (Fig. 4B). Coracoids are medium or large-sized and slenderly built. The pars epicoracoidalis is almost completely missing in all specimens except for RGM 452108 (Fig. 4B). The anterior margin is deeply concave, whereas the posterior one is straight. The pars glenoidalis is much thicker than the middle part of the bone and more or less as wide as the laminar pars epicoracoidalis.

Scapulae (Fig. 4C, D). All scapulae are medium to small, missing part of the crista anterior and of the medial end. These bones (Fig. 4C, D) are mediolaterally short, with a wide pars suprascapularis. The pars glenoidalis is preserved and the articular surface faces ventrally (Fig. 4D). The posterior margin is strongly concave. The anterior margin hosts a very well-developed crista anterior.

Humeri (Fig. 4E–G). Most of the humeri are well preserved, large and well ossified. Some specimens are smaller and more fragmentary. The humeri have a long and straight shaft, provided with a well-developed crista ventralis and a distinct crista paraventralis. The eminentia capitata is spherical and slightly shifted laterally (Fig. 4E, G). At its sides, a strong epicondylus ulnaris (medially) and a smaller, but marked, epicondylus radialis are visible. Both cristae medialis and lateralis are present. The latter is low, whereas the former is more developed and reaches up to about midshaft. The crista medialis is not strongly bent posteriorly; only in RGM 451650 (Fig. 4E–G) and 455304, it shows a clear angle at the margin close to the proximal limit, whereas in other specimens it is regularly gently curved instead. A shallow fossa cubitalis ventralis is present, closed on both sides. On the dorsal surface of the distal end, the olecranon scar is poorly marked and roughly as long as it is wide (Fig. 4E).

Radioulnae (Fig. 4H, I). MGPT-PU 138925 (Fig. 4H, I) is a very large and robust radioulna. Only a small portion of the distal end is eroded. The bone is mediolaterally compressed (except for the proximal end) and evidently constricted at the collum antebrachii. The distal end is more expanded than the proximal one. At the proximal end, the articular surface with the humerus is wide. The olecranon is thick, but rather short (its length is roughly half as the total width of the proximal end in lateral/medial view). At the distal end, the radial portion is larger than the ulnar one; this is mostly because, in distal view, the radial portion expands in medial direction. On both the lateral and medial surfaces of the bone, the radial and ulnar portions are separated by wide sulci longitudinalis, visible on the distal half of the radioulna; the sulcus is much shallower on the lateral surface, which is almost flat. Other radioulnae are either of the same size or smaller, but they share the same morphology.

Ilia (Fig. 4J, K). The ilia reach medium to large, and even very large sizes. The best-preserved ones are composed of the iliac body and part of the shaft; none is complete, but RGM 451211 (Fig. 4J, K) only misses the anterior tip of the shaft. The ilia have a wide acetabular fossa, which is subcircular in outline. Both the dorsal and ventral acetabular expansion are well developed, but the dorsal one to a higher extent. The dorsal acetabular expansion is complete only in DSTF-GH 283 and RGM 451211 (Fig. 4J, K), being very long and pointed. Anteriorly, there is a low dorsal crest on the shaft, continued posteriorly in a poorly marked and slender dorsal tubercle (distinction of the tubercle increases in the largest specimens). The tubercle is strongly inclined, dorsally curved, and it originates a very wide angle with the dorsal acetabular expansion (Fig. 4J). Anteroventral to the tubercle, the fossula tuberis superioris is not strongly marked. Posterior to the tubercle, a small and shallow supracetabular fossa is present. A marked interiliac groove and a small interiliac tubercle are present medially. The ilioischiatic juncture is high and narrow.

Ischia (Fig. 4L). The ischia are extremely large, with an overall subelliptical outline in lateral view. The bone is very robust and well ossified. It is anteroposteriorly short, with a length of about half the total height. On each side (Fig. 4L), the acetabular fossa protrudes prominently laterally, but it makes up only a small portion of the lateral surface. Based on the presence of a clear articular surface ventrally, the pubis was not ossified. In anterior view, dorsal to the acetabular fossae, there is a wide cavity facing anteriorly.

Femurs (Fig. 4M). RGM 452460 (Fig. 4M) and 452093 are very large and robust, complete or almost complete femurs, respectively, whereas other femurs only preserve the proximal or distal portions. All femurs are distinctly curved, with a sigmoid shape in the complete bone. The distal end is stocky, much thicker compared to the slenderer shaft and slightly wider than the proximal end. A low crista femuris is present proximally.

Tibiofibulae (Fig. 4N–Q). None of the tibiofibulae is complete. Nevertheless, overall, they allow a description of the complete element in this frog, because both the proximal (e.g. MGPT-PU 138931; Fig. 4N, O) and distal (e.g. MGPT-PU 139996; Fig. 4P, Q) portions are available. The bone is large, long and proportionally slender, with only a shallow expansion at the two ends (the distal end to a slightly higher degree than the proximal one). In dorsal/ventral view, the bone is straight, with a shallow concave fibular margin. The shaft is pierced by the foramen nutritium on both the dorsal and ventral sides. Shallow sulci proximalis and distalis are visible close to the respective ends. The proximal end is more compact, with a less compressed appearance than the distal one. The tibial and fibular articular surfaces are elliptical, with vertical main axis, in proximal view. A low crista cruris is present (Fig. 4O). The articular surfaces at the distal end are subcircular, and the fibular portion is slightly larger than the tibial one.

Tibial bones (Fig. 4R, S). Incomplete tibial bones (tibiale) are present, together with a single complete one (RGM 1286490; Fig. 4R, S). Most are large, but DSTF-GH 353 is much smaller and more gracile. Almost all the incomplete ones miss the distal end, but DSTF-GH 131 and 353 preserve a larger part of the shaft. RGM 451648 and 1286491 are the only specimens preserving the distal half alone. These bones are straight, elongated and slender, with enlarged ends. The proximal end is very thick compared to the shaft, whereas the distal end is laminar. The proximal end displays a wide and triangular articular surface for the related fibulare on the posteromedial surface (Fig. 4R). On the anterior surface, a sharp longitudinal ridge is visible at the proximal end, close to the lateral margin of the bone (Fig. 4S).

Remarks. Identification of a large *Latonia* frog in the Gargano material is straightforward, based on several diagnostic characters observed on the above-described fossils. Diagnostic features supporting this attribution are the following (see Roček 1994, 2013; Biton et al. 2013, 2016; Sorbelli et al. 2025): presence of a pustular sculpturing, secondarily ossified (exostosis), on dermal skull bones (most notably, the frontoparietal, but also maxillae, nasal, and squamosals); presence of the processus palatinus (originated by the fusion of the palatine bone) on the maxilla; maxilla with a long and slender processus pterygoideus and a large posterior depression (more marked in larger specimens, i.e. older individuals); completely fused frontoparietal with separated incrassatio frontoparietalis and developed pars contacta, running anteroposteriorly from anterior horns to the margo prooticum; presence of a prominentia ducti semicircularis posterioris; striations on the respective articular surfaces of the frontoparietal with the sphenethmoid and the prootic; double processes of the angulars. Other fossils mainly display features shared with other discoglossids (Bailon 1999; Roček 2013), but the overall size and robustness suggest referral to the same large *Latonia*; these include: atlases with a ventral ridge; opisthocoelous trunk vertebrae with transverse processes located ventral to the prezygapophyses; sacral vertebrae with an anterior condyle and moderately expanded transverse processes; bicondylar sacro-urostylar articulation; urostyles with small transverse processes and a dorsal longitudinal opening; short scapulae with a well-developed crista anterior; humeri with both a shifted eminentia capitata and a crista paraventralis. Attribution to the same taxon of premaxillae, ribs, the clavicle fragment, coracoids, radioulnae, ischia, femurs, tibiofibulae, and tibial bones is based on the size and robustness, as well as the shared morphology with the respective bones as figured for *Latonia* by Roček (1994), Biton et al. (2016), and Sorbelli et al. (2025). The extensive sculpturing covering cranial bones and in particular extending onto the maxillae indicates that the Gargano *Latonia* belongs to the *Latonia seyfriedi* species complex, as recently defined by Sorbelli et al. (2025). Taxonomy within this species complex is clearly in need of a clarification: current consensus sees *L. seyfriedi* as the only valid species (Syromyatnikova et al. 2019; Sorbelli et al. 2025), but species long considered synonymous with the latter should be revaluated (e.g. *Latonia kolebabi* Špinar, 1976; see discussion in Sorbelli et al. 2025) and character distribution suggests a certain degree of additional complexity might be involved (e.g. variation in posterior extension of tooth row, length of the prominentia ducti semicircularis posterioris, and inclination of sacral transverse processes in fossils previously attributed to *Latonia gigantea* (Lartet, 1851); Syromyatnikova and Roček 2019). Fossils from the Late Miocene of Gargano add to this complexity. In general, relevant diagnostic features for *Latonia* species in the Gargano fossils agrees with the conditions observed in at least some members of the *L. seyfriedi* species group, but a certain variation is present, similar to the one observed in specimens previously referred to *L. gigantea* (currently, this species is considered a junior subjective synonym of *L. seyfriedi*; Syromyatnikova et al. 2019). Variation is in some cases evident even in specimens coming from the same fissure: in prootic-exoccipitals from Chirò 12, for example, the ridge on the posterior surface is either absent (RGM 451488) or present, and when present it could be either sigmoid (RGM 451487) or straight (RGM 451484 to 451486). Presence/absence and shape of this ridge were recently discussed as potentially diagnostic within *Latonia* as a whole by Sorbelli et al. (2025), but more work to elucidate their taxonomic value is clearly needed. The same holds true for the other variable diagnostic features of *Latonia*, and thus for the time being we avoid a clear referral at species rank for the Gargano painted frog.

Family Hylidae Rafinesque, 1815
Genus *Hyla* Laurenti, 1768
***Hyla arborea* (Linnaeus, 1758)**

Hyla* gr. *arborea
Fig. 5

Material. ***Biancone 2*:** one trunk vertebra and three ilia. ***Bosco 3*:** one ilium. ***Cantatore 3A*:** three trunk vertebrae, one sacral vertebra, two urostyles, two scapulae, two humeri, and three ilia. ***Chirò 9*:** one trunk vertebra and one ilium. ***Chirò 28*:** one humerus. ***F15*:** one humerus. ***F15 err.*:** one sacral vertebra and one coracoid. ***Pirro 80/1*:** one ilium. ***Pizzicoli IV*:** one ilium.

Descriptions. ***Trunk vertebrae*** (Fig. 5A–E). The trunk vertebrae (Fig. 5A–E) are small and gracile. The neural canal is wide. The transverse processes are laminar and clearly located posterior to the prezygapophyses (Fig. 5B). The centrum is procoelous, poorly individualized and dorsoventrally depressed (Fig. 5A). The neural arch is anteroposteriorly short and has a flat and smooth dorsal surface, devoid of carina neuralis (Fig. 5B). The zygapophyses are small and subelliptical.

Sacral vertebrae (Fig. 5F–J). The sacral vertebrae are small. DSTF-GH 334 (Fig. 5F–J) is almost complete except for the right transverse process. These vertebrae have one anterior cotyle (Fig. 5F) and two posterior condyles (Fig. 5J); all of these are subelliptical, with the posterior condyles closer to subcircular. The latter are also separated by a small median gap. The neural arch defines a subelliptical neural canal. Dorsally, the arch is devoid of a carina neuralis, but it presents an arched ridge running semiparallel to the posterior margin (Fig. 5G). Only the left prezygapophysis is preserved in both specimens, being wide and subcircular. The left transverse process of DSTF-GH 334 (Fig. 3G, I) is moderately extended anteroposteriorly, fan-shaped and symmetrical (i.e. it extends to the same degree anteriorly and posteriorly).

Urostyles (Fig. 5K–P). These bones are small, gracile, straight and provided with a low carina neuralis, which is incompletely ossified dorsally (i.e. a median unsutured line is still visible in both specimens; Fig. 5L, O). There are no transverse processes, but low anteroposterior laminae are present at least in RGM 453240 (Fig. 5K–M). Anteriorly, there are two small and circular fossae condyloideae, which are clearly separated medially (Fig. 5K, N). Only in RGM 1286487 (Fig. 5N–P), a short and rounded processus intercondylicus is present ventrally between the fossae.

Coracoid (Fig. 5Q). This very small coracoid is gracile and has a straight and symmetrical morphology, with similar expansion of the two ends (but the lateral one is slightly damaged). The medial end is much more robust than the middle portion and especially than the laminar lateral end.

Scapulae (Fig. 5R, S). Scapulae are damaged but small in size and gracile. They are clearly slenderly built, with a narrow main body and a ventrally directed cavitas glenoidalis. There is no crista anterior. Most of the two ends are missing, preventing further description.

Humeri (Fig. 5T–V). The humeri are small, gracile and well ossified. The shaft is straight and devoid of a crista paraventralis. The crista ventralis is visible and moderately developed. At the distal end, the spherical eminentia capitata is shifted laterally (Fig. 5T, V). The eminentia is flanked by a proportionally large and completely ossified epicondylus ulnaris and a small epicondylus radialis. Proximally, it is bordered by a shallow fossa cubitalis ventralis. Low and almost symmetrical cristae lateralis and medialis are present. The olecranon scar is very poorly marked on the dorsal side of the humerus (Fig. 5V).

***Ilia*.** Ilia (Fig. 5W, X) are rather small and gracile, with no dorsal crest on the shaft and a bulbous and rounded dorsal tubercle, which projects laterally. The acetabular fossa is proportionally small and subtriangular. The dorsal acetabular expansion is short and pointed. There is no supracetabular fossa. The ventral acetabular expansion is well developed; anteriorly, it extends into a laminar anteroventral expansion of the preacetabular region (Fig. 5W). The medial surface of the iliac body is smooth (Fig. 5X). The ilioischiatic juncture is high and very narrow.

Remarks. Attribution of these fossils to *Hyla* tree frogs is supported by several characters presented by, e.g., Gleed-Owen (1998) and Bailon (1999). The trunk vertebrae are procoelous, with a short neural arch, no carina neuralis, and transverse processes located posterior to the prezygapophyses. The sacral vertebrae display an anterior cotyle, moderately extended transverse processes, and no carina neuralis. The urostyles are devoid of transverse processes, and they display two well-separated fossae anteriorly (i.e. the sacro-urostylar articulation is bicondylar) and a low carina neuralis. The coracoid is small and symmetrical. The scapulae are elongated, narrow and they bear no crista anterior; in addition, their cavitas glenoidalis faces ventrally. The humeri show a straight shaft, no crista paraventralis, a laterally-shifted eminentia capitata, a shallow fossa cubitalis ventralis, and visible and symmetrical cristae lateralis and medialis. Ilia bear no dorsal crest, a marked dorsal tubercle that develops laterally, and an anteroventrally expanded preacetabular region. Moreover, all bones are small and gracile, as is typical for bones of European tree frogs. Two unusual features for hylids are observed on the urostyles: i.e. the unfused suture line dorsally, and (only on RGM 1286487) the processus intercondylicus. The dorsally open neural arch is present in discoglossid urostyles (for *Discoglossus* Otth, 1837, see Bailon 1999; for *Latonia*, Biton et al. 2016) and rarely in other anurans (see e.g. Špinar et al. 1993). On the other hand, the processus intercondylicus is considered as diagnostic for palaeobatrachids by Špinar (1972), even though it might occur seldomly in other clades as well (again, see Špinar et al. 1993). However,



Figure 5. *Hyla* gr. *arborea* from the Late Miocene of the Gargano Terre Rosse. **A–E.** Trunk vertebra (RGM 452330) in anterior (**A**), dorsal (**B**), left lateral (**C**), ventral (**D**) and posterior (**E**) views; **F–J.** Sacral vertebra (DSTF-GH 334) in anterior (**F**), dorsal (**G**), right lateral (**H**), ventral (**I**) and posterior (**J**) views; **K–M.** Urostyle (RGM 453240) in anterior (**K**), dorsal (**L**) and ventral (**M**) views; **N–P.** Urostyle (RGM 1286487) in anterior (**N**), dorsal (**O**) and ventral (**P**) views; **Q.** Left coracoid (DSTF-GH 351) in ventral view; **R, S.** Left scapula (RGM 453254) in dorsal (**R**) and ventral (**S**) views; **T–V.** Left humerus (DSTF-GH 247) in ventral (**T**), medial (**U**) and dorsal (**V**) views; **W, X.** Right ilium (MGPT-PU 138902) in lateral (**W**) and medial (**X**) views.

these two urostyles cannot pertain to either of these two anuran families: discoglossid urostyles bear transverse processes (Bailon 1999), whereas palaeobatrachids have mediolaterally expanded fossae condyloideae and more developed laminae on the sides (Špinar 1972; Villa et al. 2016; A.V., pers. obs.). Because of this, we here prefer an attribution of these bones to the same hylid as the rest of the fossils; whether these characters can be explained by pathological origin, some kind of individual variation, or might bear some taxonomic value should wait for more material to be discovered prior to being settled. Discrimination at species rank of European Cenozoic tree frogs is considered impossible by several authors (Sanchiz and Mlynarski 1979; Sanchiz and Sanz 1980; Sanchiz 1981; Bailon 1999), and occurrences from the Neogene and Quaternary are often referred to more generally as members of the *H. arborea* species group (*sensu* Birbele et al. 2023). We here tentatively assign the Gargano tree frog to the same complex.

Family Bufonidae Gray, 1825
Genus *Bufotes* Rafinesque, 1815
***Bufotes viridis* (Laurenti, 1768)**

aff. *Bufotes* gr. *viridis*
Figs 6, 7

Material. ***Biancone 1*:** one trunk vertebra, one sacral vertebra, and one ilium. ***Biancone 2*:** two trunk vertebrae and one scapula. ***Bosco 2*:** three trunk vertebrae and one ilium. ***Cantatore 3A*:** six trunk vertebrae, one sacral vertebra, two urostyles, one humerus, one ilium, and two femurs. ***Chirò*:** one atlas fused with the second and third trunk vertebrae. ***Chirò 3*:** one atlas, three trunk vertebrae, one scapula, and one ilium. ***Chirò 7A*:** three trunk vertebrae, one scapula, and one ilium. ***Chirò 12*:** one trunk vertebra. ***Chirò 14*:** one trunk vertebra and one ilium. ***Chirò 28*:** three trunk vertebrae. ***F15 err.*:** one scapula. ***F21b*:** one trunk vertebra. ***F23*:** one trunk vertebra and one humerus. ***F32/4*:** one coracoid. ***Gervasio 5*:** one sacral vertebra, one urostyle, and two ilia. ***I Tre Fossi 21a*:** two trunk vertebrae and one ilium. ***Pirro 80/1*:** one ilium. ***Pizzicoli*:** one trunk vertebra and two ilia. ***Pizzicoli 1/2007*:** one ilium. ***Pizzicoli 11*:** two humeri and one ilium. ***Pizzicoli 2/2003*:** one trunk vertebra. ***Pizzicoli II*:** one trunk vertebra and one ilium. ***Pizzicoli IV*:** four trunk vertebrae. ***Rinascita 1*:** one sacral vertebra. ***San Giovannino*:** one trunk vertebra and one scapula. ***San Giovannino F2 parte bassa*:** one sacral vertebra and two coracoids. ***Tre Fossi 2A*:** one frontoparietal fused to the prootic-exoccipital, three trunk vertebrae, and four ilia.

Descriptions. ***Frontoparietal fused to prootic-exoccipital*** (Fig. 6A, B). RGM 453449 (Fig. 6A, B) is a moderately large and robust element, composed of a partial right frontoparietal fused to the underlying prootic-exoccipital. The preserved frontoparietal portion has a flat and smooth dorsal surface, a straight margo sagittalis, and a long and deep occipital canal with an anterolateral course (Fig. 6A). The prootic-exoccipital misses most of the crista prootica. The damage complicates observing the course and placement of the postorbital ridge, but it could be estimated to run more posteriorly than laterally and not being located along the anterior margin of the prootic. Most of the rest of the prootic-exoccipital is also quite damaged, preventing a satisfactory and informative description.

Atlas (Fig. 6C–G). The isolated atlas is small but robust. It has a strongly dorsoventrally compressed centrum, with a posterior condyle (Fig. 6D). Anteriorly, the cotyles are wide and only slightly inclined dorsolaterally (Fig. 6C). They are separated medially by a short gap. In anterior view, the neural canal is subcircular, but very slightly depressed. Dorsally, the carina neuralis is almost indistinct (Fig. 5E). Ventral to the postzygapophyses, the wall of the neural arch originates a short posterior expansion (subzygapophyseal spine *sensu* Bailon 1999), which is preserved only on the right side (Fig. 5F).

Fused atlas*, *second and third trunk vertebrae (Fig. 6H–L). MGPT-PU 138950 represents a complex including the atlas, the second and the third vertebrae, all fused together. Limits between the bones are obliterated in almost all cases, but the presence of three vertebrae is supported by the two pairs of transverse processes after the atlas (Fig. 6J, K). The neural arches are badly damaged, but they are clearly short and provided with a carina neuralis (Fig. 6J). The carina itself is only preserved on the second vertebra, being clearly low and thick. The transverse processes are cylindrical and laterally directed. The fused vertebral centra are strongly dorsoventrally compressed and have a smooth ventral surface (Fig. 6K). A foramen is present in the middle, at the level of the joint between the atlas and the second vertebra. The posterior end is damaged, not really allowing stating whether a posterior cotyle or condyle was present. Anteriorly, the two cotyles for the articulation with the skull (fossae condyloideae) are narrow, mediolaterally elongated and bend dorsolaterally by the sides (Fig. 6H); medially, they merge together, with no spatium interglenoidale. The neural canal is wide; the damage at the roof of the neural arch complicates the evaluation of the shape of the canal, but it was likely ogival.

Trunk vertebrae (Fig. 6M–Q). These procoelous trunk vertebrae (Fig. 6M–Q) are small to medium-sized but robust, with thick lateral walls and a well-individualized centrum. Overall, the surfaces of the vertebrae have a rough appearance, with small pits and striations visible in some points. The cotyle and condyle are subelliptical, slightly dorsoventrally compressed (most cases), or strongly compressed (MGPT-PU 138908, DSTF-GH 231 and 343, RGM 451282, 451283, 451498, 451566, 453445, 454620 and 454621). The neural canal is subpentagonal (most specimens), reniform (MGPT-PU 138908, 139991 and 142660, DSTF-GH 231, and RGM 453445) or subcircular (DSTF-GH 343 and RGM 451498) in anterior view. The neural arch is short; generally, it has a low and distinct carina neuralis dorsally. The carina becomes more robust in the posterior half, and it projects short posteriorly with a very minute point. Only the specimens with a strongly compressed centrum have a more robust carina for the whole length of the arch (Fig. 6O), with a subtriangular or widely subquadrangular morphology in dorsal view. This, together with the other differences shown by these vertebrae, suggests that they represent one of the first vertebrae following the atlas. Only MGPT-PU 139991 and 142660, which likely represent very young individuals (M.D. & A.V., pers. obs. on MGPT MDHC individuals), have a slightly longer and dorsally flat neural arch, with no carina neuralis and no posterior point. The transverse processes are wide and either laminar or more robust, located posterior to the prezygapophyses. The zygapophyses are weakly individualized from the neural arch and subcircular. Again, MGPT-PU 139991 and 142660 differ: these have zygapophyses, which are well individualized and distinctly projected anterolaterally

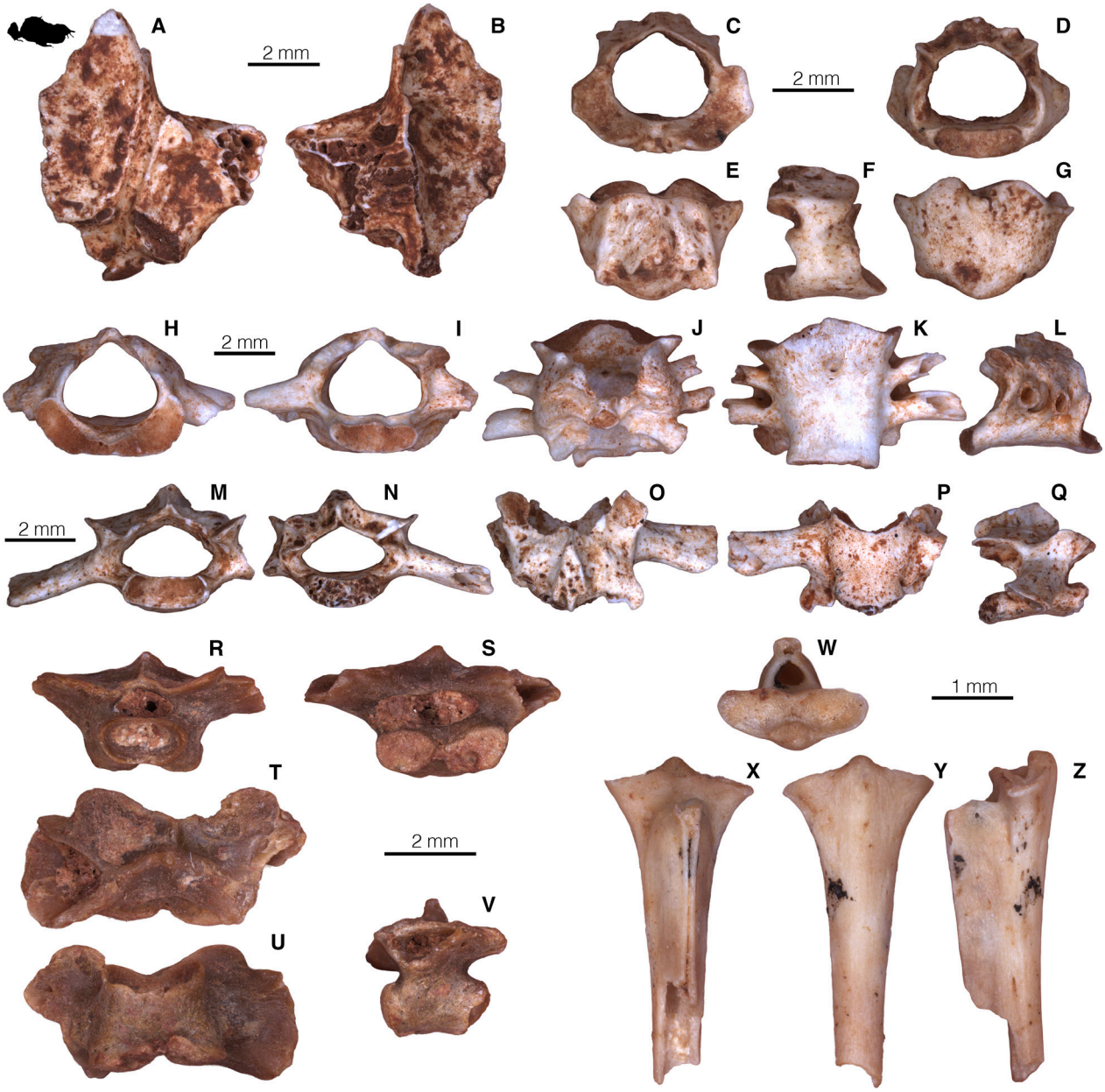


Figure 6. aff. *Bufotes* gr. *viridis* from the Late Miocene of Gargano Terre Rosse. **A, B.** Fused right frontoparietal and prootic-exoccipital (RGM453449) in dorsal (**A**) and ventral (**B**) views; **C–G.** Atlas (RGM 452039) in anterior (**C**), posterior (**D**), dorsal (**E**), right lateral (**F**) and ventral (**G**) views; **H–L.** Fused atlas, second and third trunk vertebrae (MGPT-PU 138950) in anterior (**H**), posterior (**I**), dorsal (**J**), ventral (**K**) and right lateral (**L**) views; **M–Q.** Trunk vertebra (MGPT-PU 138908) in anterior (**M**), posterior (**N**), dorsal (**O**), ventral (**P**) and right lateral (**Q**) views; **R–V.** Sacral vertebra (RGM 454244) in anterior (**R**), posterior (**S**), dorsal (**T**), ventral (**U**) and right lateral (**V**) views; **W–Z.** Urostyle (RGM 453506) in anterior (**W**), dorsal (**X**), ventral (**Y**) and right lateral (**Z**) views.

and posterolaterally, respectively for the pre- and postzygapophyses. This gives a rather elongated and thick X shape to these two vertebrae in dorsal view.

Sacral vertebrae (Fig. 6R–V). This medium-sized sacral vertebrae (Fig. 6R–V) miss most of the transverse processes and, in the case of DSTF-GH 142, part of the neural arch. The vertebrae are robustly built, with a subtrapezoidal centrum characterized by an anterior cotyle and two posterior condyles. The cotyle is subcircular in DSTF-GH 142 and elliptical in the other specimens, whereas the condyles are subelliptical in all cases. Medially, the posterior condyles are closely spaced but clearly separated (Fig. 6S). In anterior view, the neural canal is small and reniform. The neural arch is anteroposteriorly short and provided dorsally with a low crista neuralis (Fig. 6T). The prezygapophyses are wide and suboval. The transverse processes are more preserved in RGM 454244 (Fig. 6T, U): they slightly expand anteroposteriorly.

Urostyles (Fig. 6W–Z). The urostyles are moderately small. When preserved, the carina neuralis is high and still presents a narrow opening dorsally along most of its length (Fig. 6X). By the anterior end, there are no transverse processes. The two fossae condyloideae are

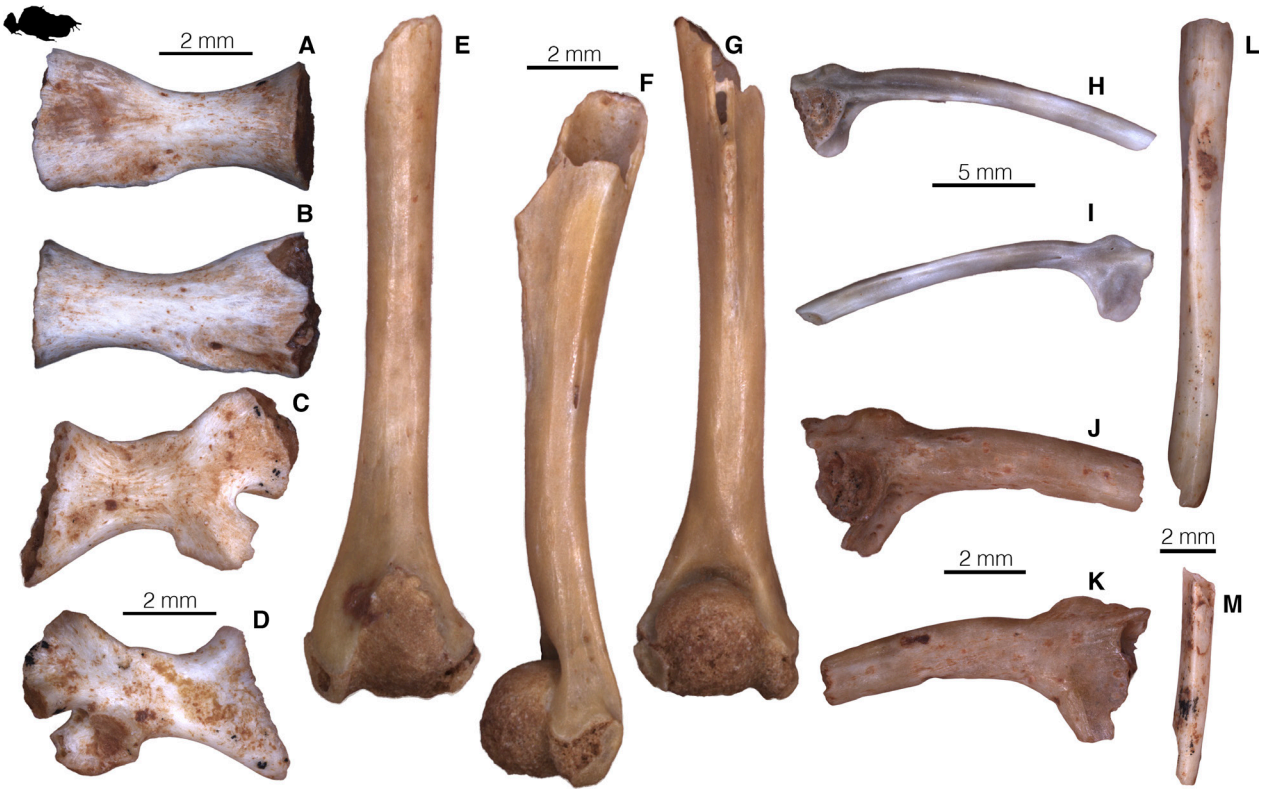


Figure 7. aff. *Bufotes* gr. *viridis* from the Late Miocene of the Gargano Terre Rosse. **A, B.** Right coracoid (DSTF-GH 346) in ventral (**A**) and dorsal (**B**) views; **C, D.** Left scapula (RGM 452109) in dorsal (**C**) and ventral (**D**) views; **E–G.** Right humerus (RGM 454370) in dorsal (**E**), medial (**F**) and ventral (**G**) views; **H, I.** Right ilium (MGPT-PU 138915) in lateral (**H**) and medial (**I**) views; **J, K.** Right ilium (DSTF-GH 164) in lateral (**J**) and medial (**K**) views; **L.** Femur (RGM 453271) in posterior view; **M.** Femur (RGM 453272) in posterior view.

mediolaterally elongated and in close contact medially, even merging in RGM 453506 (Fig. 6W). The same specimen also shows a short processus intercondylicus (Fig. 6X, Y), which is absent in the other fossils. In anterior view, the neural canal is subtriangular (Fig. 6W).

Coracoids (Fig. 7A, B). These fossils are medium-sized and distinctly robust coracoids. All are either completely or almost completely preserved. The laminar pars epicoracoidalis is only slightly more expanded than the thick pars glenoidalis. Both the anterior and posterior margins are slightly concave, the anterior one to a slightly higher degree. Overall, the coracoid is rather short, in mediolateral extension.

Scapulae (Fig. 7C, D). The scapulae are medium-sized (except for RGM 453771, which is much smaller), mediolaterally elongated and moderately robust. RGM 452109 (Fig. 7C, D) is complete, whereas both the medial and lateral ends are slightly damaged in the other fossils. The cavitas glenoidalis opens ventrally (Fig. 7D). There is no fossa supraglenoidalis. The two ends of the bone are similarly expanded. A very small anterior crest along the margo anterior is present on RGM 452109 (Fig. 7C, D) and 455144, close to the pars acromialis, but not in RGM 452181 and 453771. The pars acromialis of RGM 452109 (Fig. 7C, D) and 455144 has a rounded anteromedial outline.

Humeri (Fig. 7E–G). These humeri are medium-sized, provided with a straight (DSTF-GH 280) or curved (RGM 453256, 454370 and 454371; Fig. 7E, G) diaphysis. There is no crista paraventralis. The crista ventralis is present. The proximal end is not preserved. The distal end is damaged or poorly ossified, but the eminentia capitata is clearly shifted laterally (Fig. 7E, G). In contrast to the other specimens, RGM 453256 bears a spherical and well-ossified eminentia capitata. The fossa cubitalis ventralis is present and shallow. Both epicondyles are poorly ossified, again with the sole exception of RGM 453256. The cristae medialis and lateralis are low, only incipient in RGM 453256, 454370 (Fig. 7E–G) and 454371. On the dorsal surface, the olecranon scar is short and broad (Fig. 7E).

Ilia (Fig. 7H–K). MGPT-PU 138915 (Fig. 7H, I), DSTF-GH 164 (Fig. 7J, K), and RGM 454595 are almost complete ilia. The former two are small and rather gracile, but the latter is larger and more robust. The straight shaft is devoid of a dorsal crest. An incipient lamina calamita is present in MGPT-PU 138915 (Fig. 7H) and RGM 454595, but not DSTF-GH 164 (Fig. 7J). The body has a subcircular acetabular fossa, a short dorsal acetabular expansion, a large ventral acetabular expansion, a deep preacetabular fossa, a very shallow supracetabular fossa, and a distinct dorsal tubercle. The tubercle is bulbous and dorsally rounded, without clear lobes or with two incipient lobes (only in RGM 454595). It has to be noted, however, that a certain degree of polishing is evident on the various structures of the iliac body; it is not clear, then, how much

this could have impacted the surface of the tubercle. Medially, there are no interiliac grooves or tubercles. Other ilia are less preserved, but they share a comparable morphology. In most cases, their dorsal tubercle clearly displays a rough surface, with a pair of small lobes.

Femurs (Fig. 7L, M). The femurs are slender. RGM 453271 (Fig. 7L) is rather large, whereas RGM 453272 (Fig. 7) is much smaller. Both display a high and sharp crista femoris, which shows no clear sign of splitting.

Remarks. Bufonid remains in the Gargano material are also represented by several bones, mainly from the postcranium. Characters supporting assignment to this anuran family includes (Gleed-Owen 1998; Bailon 1999; Roček 2013): paired frontoparietal with an occipital canal; occasional fusion of the first vertebrae; posterior condyle and dorsoventrally compressed centrum of the atlas; procoelous vertebrae with a short neural arch, strong lateral walls, and transverse processes posteroventral to the prezygapophyses; anterior cotyle, moderately expanded transverse processes, and crista neuralis of the sacral vertebrae; urostyles with two elongated fossae condyloideae, a high carina neuralis, and devoid of transverse processes; robust coracoids with slightly asymmetrical ends; robust scapulae elongated and provided with a cavitas glenoidalis facing ventrally; humerus with no crista paraventralis, but with a shifted eminentia capitata, a fossa cubitalis ventralis, and low but distinct cristae medialis and lateralis; uncrested ilia with a dorsal tubercle and a short dorsal acetabular expansion; high crista femoris. Identification below family rank is complicated by somehow mixed indications given by some of the elements. Several bones clearly show morphological features supporting referral to *Bufotes* with a certain degree of confidence, including (Sanchiz 1977; Bailon 1999; Ratnikov 2001; Blain et al. 2010): the ogival neural canal and the mediolaterally extended and horizontal fossae condyloideae of the atlas; the presence of a subzygapophyseal spine; the absence of a fossa supraglenoidalis on the scapula and, on the same bone, the rounded outline of the pars acromialis and the rare presence of a very low crista anterior; the deep preacetabular fossa and the generally bilobed dorsal tubercle on the ilia. The presence of the lamina calamita was proposed by Sanchiz (1977) and later Bailon (1999) as diagnostic for ilia of *Epidalea calamita* (Laurenti, 1768), but an incipient version of this structure can be seldom present in other bufonids as well (Syromyatnikova 2015; Villa et al. 2020). Straightforward attribution of other bones to green toads is more complicated. As far as the fused frontoparietal and prootic-exoccipital complex is concerned, the straight margo sagittalis and the crista prootica running more posteriorly and not located along the anterior margin are *Bufotes* features, but the long and anterolaterally-directed occipital canal is found in extant *Epidalea* Cope, 1864 (Bailon 1999; Blain et al. 2010) and the extinct *Bufo mirus* Syromyatnikova, 2015 (considered a species close to *Strauchbufo raddei* (Strauch, 1876); Syromyatnikova 2015). Similarly, the urostyles are more comparable to *Bufotes* (or *Bufo* Garsault, 1764) in the subtriangular section of the neural canal, but to *Epidalea* in the medial contact between the fossae condyloideae (Bailon 1999). Moreover, and as already mentioned above for the hylids, the dorsal opening of the carina neuralis in the urostyle is unusual in non-discoglossid anurans. At least one extinct toad, *Bufotes priscus* (Špinar et al. 1993) from the Middle Miocene of Slovakia (originally assigned to *Bufo*, this species was later reallocated to *Pseudepidalea* Frost, 2006 by Martín et al. 2012, currently a junior objective synonym of *Bufotes* following Dubois and Bour 2010), displays a fissured urostyle (Špinar et al. 1993; Sanchiz 1998), indicating that this feature might be seldom present in bufonids as well. Nevertheless, the toad from Gargano cannot be referred to this species, because *B. priscus* has sculptured frontoparietal and prootic-exoccipital (Špinar et al. 1993; Sanchiz 1998). The crista femoris usually displays an incipient split in *Bufotes*, whereas it is single and sharp in *Epidalea*; however, Bailon (1999) implied variation in the condition shown by the green toads. Taking all of this into account, toad fossils from the Late Miocene of Gargano most closely resemble green toads, but showing a few differing or unusual features. Because of this, we tentatively assign them here to aff. *Bufotes* gr. *viridis*, using the particle aff. (i.e. affinis) in the sense explained by Sigovini et al. (2016) to account for these few differences. Here, the *B. viridis* species group includes all species related with *B. viridis* s.l. by Blain et al. (2010). In contrast with previous accounts (e.g. Savorelli et al. 2025), we found no clear evidence of *Bufo* s.s. in the studied material.

Family Ranidae Batsch, 1796
Genus *Pelophylax* Fitzinger, 1843

Pelophylax sp.

Fig. 8

Material. ***Biancone 2*****:** one humerus. ***Cantatore 3A*****:** one ilium. ***Chirò*****:** one maxilla. ***Chirò 3*****:** two angulars, three trunk vertebrae, one sacral vertebra, one urostyle, and one coracoid. ***Chirò 15*****:** one humerus. ***F9*****:** one trunk vertebra. ***F15 err.*****:** one trunk vertebra and two ilia. ***F23*****:** one trunk vertebra. ***F32/10*****:** one ilium. ***Fina D*****:** one sacral vertebra, one scapula, two humeri, and two ilia. ***Pizzicoli IV*****:** one sacral vertebra and two ilia.

Descriptions. ***Maxilla*** (Fig. 8A, B). MGPT-PU 138964 is a medium-sized maxilla, preserving the anterior half of the bone. It is slender and lightly built, with a moderately developed lamina horizontalis ending with a thickened medial margin (Fig. 8B). The crista dentalis hosts closely packed tooth positions; these are almost completely empty, but the teeth were pleurodont, pedicellate, slender and cylindrical. The anterior end of the maxilla bears a short rostellum. The dorsal margin of the maxilla is damaged. The basis of the processus palatinus is visible, but the processus itself is almost completely broken off; it was likely laminar. The lateral surface of the maxilla is smooth (Fig. 8A).

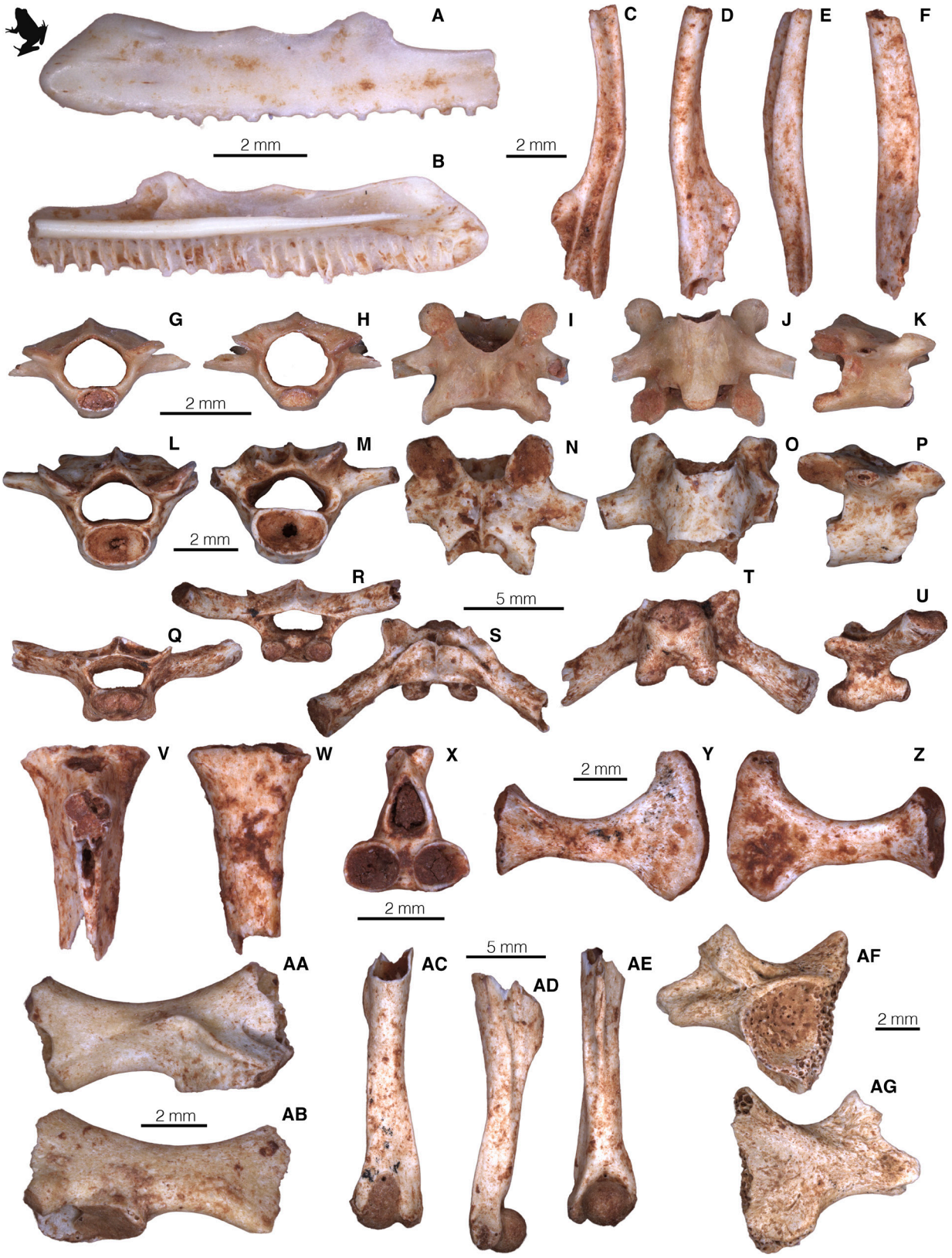


Figure 8. *Pelophylax* sp. from the Late Miocene of the Gargano Terre Rosse. **A, B.** Left maxilla (MGPT-PU 138964) in lateral (**A**) and medial (**B**) views; **C–F.** Right angular (RGM 452072) in dorsal (**C**), ventral (**D**), lateral (**E**) and medial (**F**) views; **G–K.** Trunk vertebra (DSTF-GH 333) in anterior (**G**), posterior (**H**), dorsal (**I**), ventral (**J**) and right lateral (**K**) views; **L–P.** Trunk vertebra (DSTF-GH 175) in anterior (**L**), posterior (**M**), dorsal (**N**), ventral (**O**) and right lateral (**P**) views; **Q–U.** Sacral vertebra (RGM 452045) in anterior (**Q**), posterior (**R**), dorsal (**S**), ventral (**T**) and left lateral (**U**) views; **V–X.** Urostyle (RGM 452100) in dorsal (**V**), ventral (**W**) and anterior (**X**) views; **Y, Z.** Left coracoid (RGM 452061) in dorsal (**Y**) and ventral (**Z**) views; **AA, AB.** Left scapula (RGM 453926) in dorsal (**AA**) and ventral (**AB**) views; **AC–AE.** Left humerus (RGM 451627) in dorsal (**AC**), medial (**AD**) and ventral (**AE**) views; **AF, AG.** Left ilium (DSTF-GH 218) in lateral (**AF**) and medial (**AG**) views.

Angulars (Fig. 8C–F). The angulars are slender and medium sized. The anterior tip is regularly missing, and the extremitas spatulata is damaged. The sulcus pro cartilago Meckeli is shallow all along the bone. The processus coronoideus is single and mediodorsally oriented. In dorsal view (Fig. 8C), the same process is elongated and short and displays a gently convex medial outline.

Trunk vertebrae (Fig. 8G–P). The trunk vertebrae are medium-sized and amphicoelous (DSTF-GH 175 and 282, RGM 452042; Fig. 8L–P) or procoelous (other specimens; Fig. 8G–K). In the amphicoelous vertebrae, the centrum is subcylindrical, slightly dorsoventrally compressed and pierced anteroposteriorly by a notochordal foramen (Fig. 8L, M). Other vertebrae have a more dorsoventrally compressed centrum, which is less individualized from the rest of the arch (Fig. 8G, H). The neural canal is subelliptical. The short neural arch has thin lateral walls and a flat dorsal surface, with a low carina neuralis running in the middle (Fig. 8I, N). The zygapophyses are wide and subcircular. The transverse processes are laminar, located posterior to the prezygapophyses and directed laterally.

Sacral vertebrae (Fig. 8Q–U). The sacral vertebrae are medium-sized. The bones are moderately robust and rather well preserved, with the most complete one, RGM 452045 (Fig. 8Q–U), missing only the right prezygapophysis and the distal end of the right transverse process. Anteriorly, the vertebra has a wide and subelliptical condyle. Posteriorly, there are two condyles, which are small, subcircular and well separated medially (Fig. 8R). The centrum is dorsoventrally depressed. The neural canal is elliptical in anterior and posterior views. The short neural arch bears a low but distinct carina neuralis (Fig. 8S). At mid-length of this carina, a curved ridge develops posterolaterally on each side, ending at the basis of each transverse process. The latter processes are posterolaterally directed and cylindrical. The prezygapophyses are moderately wide and subcircular.

Urostyle (Fig. 8V–X). The only available urostyle is a poorly preserved fragment, represented just by the anterior end. The fossil is medium sized. Anteriorly, it presents two small and circular fossae condyloideae (Fig. 8X), with a short gap between them. The carina neuralis is high and devoid of transverse processes. The crista is mostly broken off, but the anterior end is mediolaterally expanded (Fig. 8V, X). The canalis coccygeus is subtriangular in anterior view (Fig. 8X).

Coracoid (Fig. 8Y, Z). The coracoid is medium-sized and slender. In dorsal view, it is strongly asymmetrical, with the laminar pars epicoracoidalis almost twice as wide as the more robust pars glenoidalis. Still in the same view, the margo anterior is strongly concave, whereas the margo posterior is shallowly concave.

Scapula (Fig. 8AA, AB). The scapula is medium in size and elongated. The cavitas glenoidalis opens in posterior direction (Fig. 8AB). Both the pars suprascapularis and pars acromialis are damaged. Anteriorly, there is no crista anterior, and the margo anterior is thus distinctly concave. A ridge is present on the dorsal surface of the scapula (Fig. 8AA), running on the pars glenoidalis and only to a limited extent over the body of the bone.

Humeri (Fig. 8AC–AE). RGM 451627 (Fig. 8AC–AE) is a moderately large and slenderly built humerus. The shaft is straight. The eminentia capitata is spherical and placed in line with its main axis (Fig. 8AC, AE). There is no crista paraventralis, whereas the crista ventralis is well developed. The crista medialis is slightly more developed than the almost indistinct crista lateralis. Moreover, the crista medialis does not bend dorsally and reaches up to about halfway through the shaft (Fig. 8AD). The fossa cubitalis ventralis is deep. The epicondyles are distinct, with the ulnaris one being much more developed than the small radialis one. The olecranon scar is well marked and elongated (Fig. 8AC). The other three humeri are morphologically similar but smaller and less preserved. RGM 453922, in particular, is much smaller and lacks the cristae medialis and lateralis.

Ilia (Fig. 8AF, AG). The large ilia preserve the iliac body and the most proximal part of the shaft. On the lateral side, they have a large and subcircular acetabulum, defined by a distinct rim. The dorsal acetabular expansion is robust, but the distal tip is missing in all specimens, preventing an evaluation of the overall development. The ventral acetabular expansion is not distinctly developed. The shaft bears a high and vertical dorsal crest. The dorsal tubercle, merged with the proximal end of the crest, is also vertical and well developed, with well-marked margins and a smooth lateral surface (Fig. 8AF). The angle defined by the tubercle and the dorsal acetabular expansion is close to 90°. A shallow supracetabular fossa is visible. On the other hand, there is no preacetabular fossa. The medial surface of the ilium is smooth, devoid of interiliac tubercle and groove. When preserved, the ilioischiatic juncture is high and moderately thick.

Remarks. The following combinations of characters support the identification of ranid remains in the Gargano material (Gleed-Owen 1998; Holman 1998; Bailon 1999; Ratnikov 2001): medium-sized, slender and toothed maxilla without developed processus palatinus or sculpturing; slender angulars with mediodorsally directed processus coronoideus; amphicoelous or procoelous trunk vertebrae, with a short neural arch, thin lateral walls, a low carina neuralis, laterally-directed transverse processes located posterior to the prezygapophyses, and a poorly individualised centrum; bicotylar sacrourostylar articulation, made up by circular condyles on the sacrals and corresponding fossae on the urostyle; sacral vertebrae with an anterior condyle and cylindrical transverse processes; urostyle lacking transverse processes, but provided with a high carina neuralis; slender and strongly asymmetrical coracoid; elongated scapula with posteriorly-facing cavitas glenoidalis and a dorsal ridge; humeri with an eminentia capitata aligned with a straight shaft and no crista paraventralis; ilia with a high and vertical dorsal crest. A few remains, including the scapula, the humeri, and the ilia, allow to further refine the assignment, at least to the rank of genus, based on diagnostic characters reported by Gleed-Owen (1998), Bailon (1999), and

Ratnikov (2001). Other bones are herein attributed to the same ranid because there is currently no evidence of two different taxa being present. The ridge present on the dorsal surface of the scapula is mainly limited to the pars glenoidalis, a condition shared more with green frogs rather than with brown frogs. Similarly, the transversal crista medialis reaching up only to mid-length of the humeral shaft, the marked dorsal tubercle of the ilium originating a 90° angle with the dorsal acetabular expansion, and the high and thick ilioischiatic juncture are green frog features. Species-rank identification of green frog isolated fossils is virtually impossible with the available knowledge, and at least for ilia, it can be done only with an amount of fossils representative of the original population (Blain et al. 2015). Because of this, we cautiously identify all these remains as simply pertaining to *Pelophylax* sp.

Anura indet.

Material. ***Bosco 4*****:** one distal phalanx. ***Chirò*****:** two maxillae. ***Chirò 80/1 NL*****:** three maxillae, one urostyle, two radioulnae, and one tibiofibula. ***F1*****:** one tibiofibula. ***F9*****:** one trunk vertebra and one femur. ***F15*****:** one premaxilla, one trunk vertebra, and one radioulna. ***F15 err.*****:** three maxillae, two squamosals, one trunk vertebra, one humerus, two radioulnae, two tibiofibulae, and one phalanx. ***F21B*****:** one humerus and one femur. ***F23*****:** one tibiofibula. ***F32/2*****:** one autopodial element. ***F32/10*****:** one (tentative) autopodial element. ***F32/11*****:** one radioulna. ***Fina 2013*****:** one maxilla. ***Fina H*****:** two phalanges. ***Gervasio 5*****:** three angulars. ***I Tre Fossi 21a*****:** one tibiofibula. ***Pizzicoli*****:** one maxilla, one vertebral fragment, two femurs, and one tibiofibula. ***Pizzicoli II*****:** one (tentative) tibiale. ***Pizzicoli IV*****:** one premaxilla, one squamosal, one vertebral fragment, one urostyle, one coracoid, one humerus, two radioulnae, one ilium, two tibiofibulae, and one phalanx. ***San Giovannino F2 parte bassa*****:** one premaxilla, one coracoid, one humerus, one radioulna, one ischium, and two autopodial elements. ***San Nazario – bivio Lesina sinistra*****:** one tibiofibula. ***"Terre Rosse", locality indet.*****:** one vertebral fragment and one humerus.

Remarks. Several remains are too fragmentary or scarcely diagnostic and are herein only attributed to indeterminate anurans. Some of the radioulnae display a deep fossa just distal to the proximal end. Based on our preliminary observations on the MGPT-MDHC collection, this deep fossa seems to be absent in ranids and developed in at least some bufonids. However, this should be checked on more comparative specimens prior to being considered as a valid diagnostic feature.

Results of the distribution analysis

In general, amphibians (or better, anurans, given that no remains of urodeles were found) are scarcely represented in the Late Miocene Terre Rosse fissure fillings in Gargano (see also Suppl. material 1). NISP reached a maximum of 45 (in fissure Chirò 3), whereas MNI was regularly lower than 10 (maximum MNI = 9, in fissure Chirò 12). The mean NISP is 8.4 and the mean MNI is 2.5, for 62 fissures with anurans. *Latonia* gr. *seyfriedi* is by far the most represented anuran taxon (Fig. 9A, B), both in terms of NISP (~61%) and MNI (~60%). It is present in almost all fissures that have yielded anuran remains, with only seven out of 62 fissures (~11%) devoid of *Latonia* remains. In most cases, it is the most abundant or the only anuran identified in a fissure; cases where the *Latonia* MNI is matched by another anuran are limited to 12 fissures (about 19%) and those where another anuran is more abundant are even less: only three fissures, about 5%. The second most abundant anuran is aff. *Bufotes* gr. *viridis* (Fig. 9A, B), representing ~21% of individuals and ~16% of the remains and recovered in ~44% of the fissures (27 out of 62). Then, *Hyla* gr. *arborea* (nine fissures) and *Pelophylax* sp. (10 fissures) follow as minor components of the overall assemblage (Fig. 9A, B), both at ~5% NISP and ~8% MNI. Bufonids, hylids, and ranids are the most abundant or sole anuran identified in only a limited number of fissures: respectively, four, three and one fissures out of 62. Only 13% of the remains were referred to indeterminate anurans (Fig. 9B); these testified for the occurrence of an additional ~3% of the total MNI (Fig. 9A).

MNI-based distribution of the anuran taxa in the different phases defined by Savorelli et al. (2016, 2025) shows a similar trend, with an overrepresentation of *Latonia* in most of the phases and limited contributions by the other taxa (Fig. 9C). Only subphase 2a seems to show a more equal representation of the different Gargano anurans. However, this overall analysis of the phases must be taken with caution, due to the intrinsic limitation originating from the small number of fissures for which phase attribution is currently possible. As a matter of fact, some of the subphases are represented only by one or slightly more fissures, and even the phase with the most fissures, phase 4, only counts on 11 fissures. Thus, the picture provided by our current dataset is only preliminary and cannot be used to extrapolate clear diversity trends for the Gargano Late Miocene anurofauna, apart from the stable and relevant role played by *Latonia* in the community. Features apparent from the graph in Fig. 9C such as the less monopolised assemblage in subphase 2a, the disappearance of *Hyla* after the same subphase, and the constrained presence of *Pelophylax* between subphases 2a and 3a could be spurious and strongly biased.

Phylogenetic analysis of the Gargano *Latonia*

In our replication of both the second and third iterations of Sorbelli et al.'s (2025) analysis, our results were almost identical to those obtained by the latter authors. When *Eodiscoglossus* and *Wealdenbatrachus* are included, we

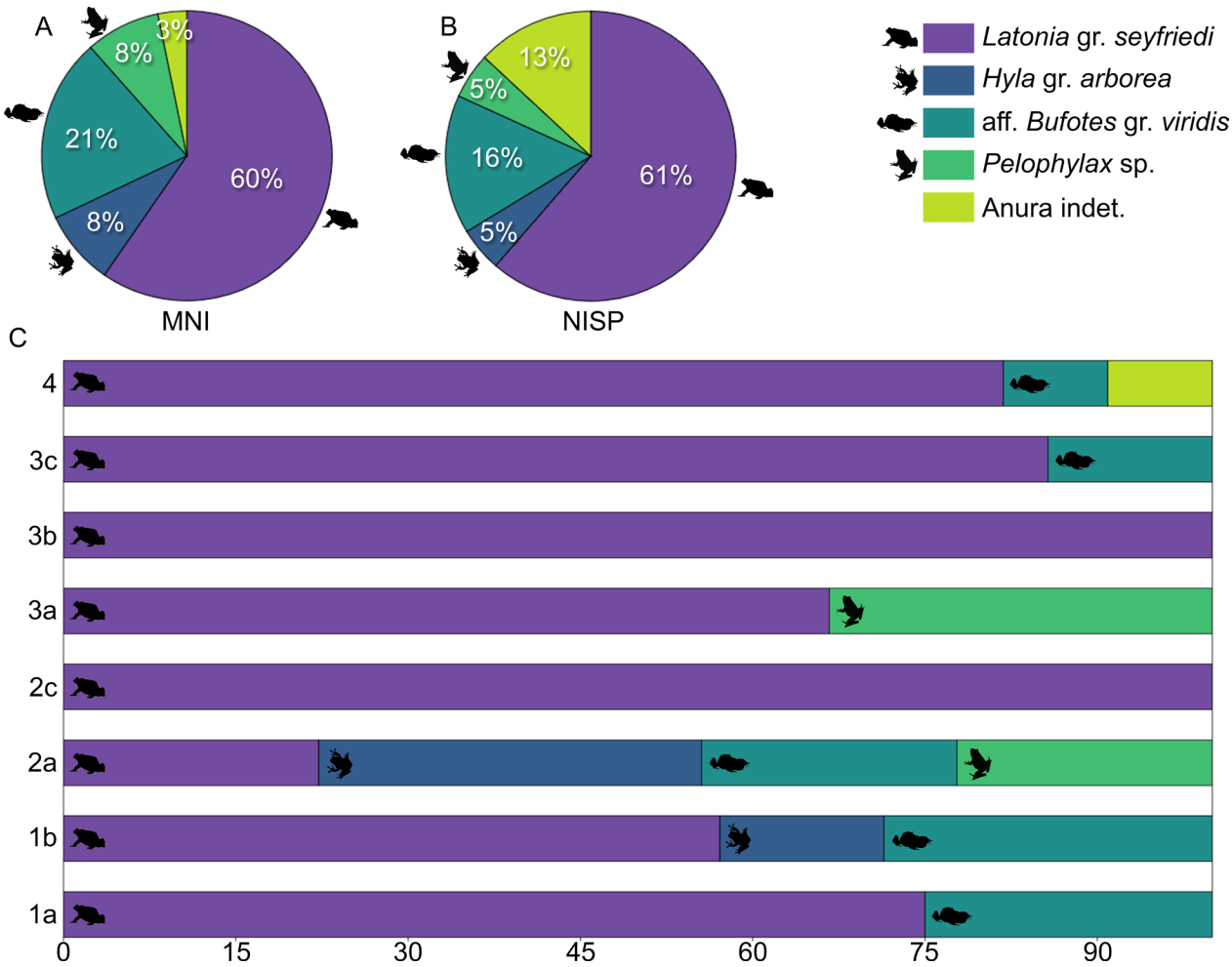


Figure 9. Distribution of anuran individuals and remains in the Gargano Terre Rosse assemblages. **A.** Distribution in the whole record, based on the minimum number of individuals (MNI); **B.** Distribution in the whole record, based on the number of identifiable specimens (NISP); **C.** Distribution in the different biostratigraphic phases of the Terre Rosse, based on the MNI.

obtained four most parsimonious trees, with a length of 60 steps. The strict consensus has a consistency index of 0.62 and a retention index of 0.77. When the two Mesozoic taxa are excluded, the run gives a single tree (Fig. 10), 54 steps long (consistency index: 0.82; retention index: 0.92). The topology of the consensus trees is the same as Sorbelli et al.'s (2025), with the only difference being of course the presence of the Gargano OTU. The latter forms a polytomy with *L. kolebabi* and *L. seyfriedi* in both iterations, thus further supporting our attribution of the Gargano material to the *L. seyfriedi* species group.

Discussion

Our survey of the large number of fossils recovered from the Gargano Terre Rosse fissures looking for amphibians resulted in the recovery of a limited number of remains: only 528 specimens, representing a minimum of 156 individuals from 62 fissures (see Suppl. material 1). This sample clearly represents an impoverished and unbalanced fauna, with only four taxa identified (*Latonia* gr. *seyfriedi*, *Hyla* gr. *arborea*, aff. *Bufotes* gr. *viridis*, and *Pelophylax* sp., plus some remains only attributable to indeterminate anurans and potentially referable to one or more of the previous taxa) and an evident dominance of the discoglossid *Latonia* (Fig. 9). This suggests that the Terre Rosse anurans could represent insular communities, in agreement with what is observed for other vertebrates from the Late Miocene of Gargano (Masini et al. 2010; Savorelli et al. 2025) and in particular with other components of the local herpetofauna (Georgalis et al. 2025). Irrespective of the degree of precision with which the Gargano anurans are identified (i.e. none of them is precisely identified at species rank), most of them display some sort of peculiar osteological feature. The Gargano *Latonia* shows significant variation in characters considered diagnostic at species rank in recent works on the genus (Syromyatnikova and Roček 2019; Sorbelli et al. 2025), and a similar mix of diagnostic characters, this time even relevant for generic attribution, is also evident in the green toads. Moreover, the urostyles of both the green toads and the tree frogs share uncommon morphological characters for these clades, including an unfused dorsal suture line and, sometimes, the presence of a processus intercondylicus (see respective Remarks). Taken all together, these

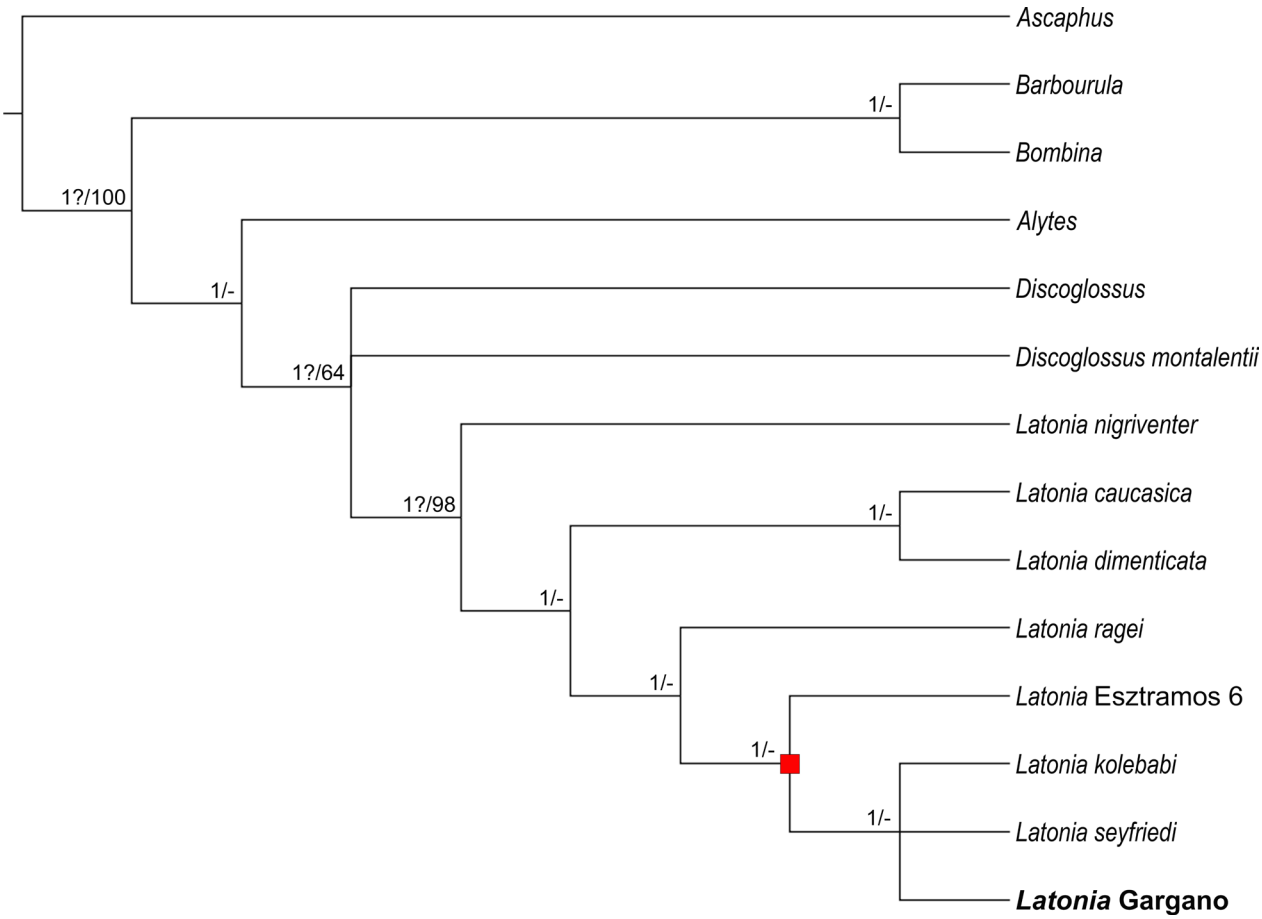


Figure 10. Phylogenetic relationships of the Gargano *Latonia*. The shown topology is based on the only tree resulting from the analysis without all taxa with less than 50% of characters scored and excluding also *Eodiscoglossus* and *Wealdenbatrachus*. The red square marks the *Latonia seyfriedi* species complex, as defined by Sorbelli et al. (2025). Bremer and bootstrap values (in this order) are provided, calculated with TNT. A question mark following the Bremer values indicates cases when the software could not run enough replications to confidently support value calculation. Bootstrap values < 50% are omitted.

peculiar morphologies might further result from evolution in insular conditions for these anurans, with diversification into potential endemic species with distinguished characters or, especially for the two taxa with a lower representation (potentially paralleling smaller actual populations on the palaeoisland), bottleneck spreading of usually rare or unusual features (Rebouças et al. 2019). Furthermore, it must be noted that the Gargano amphibian palaeofauna also agrees with the general trend observed on other Mediterranean islands, namely the absence or underrepresentation of urodeles (see Introduction).

If our assumptions on the insular characteristics of the anuran assemblages from the Gargano Terre Rosse are correct, it seems further possible that what is represented in the fossil record from the fissures is a picture of already insularized anuran palaeocommunities, and that earlier stages of the palaeoisland colonization are missing. The long history of studies on the mammals from the Terre Rosse also highlighted a similar issue, with the strong endemicity displayed by the overall Gargano palaeofauna (the so-called *Mikrotia* fauna) and its components being a long-lasting problem for both biostratigraphy and biogeography (Freudenthal 1971; Rook et al. 2006; Mazza and Rustioni 2008; Van den Hoek Ostende et al. 2009; Freudenthal and Martín-Suárez 2010; Freudenthal et al. 2013; Savorelli and Masini 2016; Savorelli et al. 2017, 2025). It must be noted, however, that amphibians from the oldest phase (phase 0, currently only represented by fissure M013; Masini et al. 2013; Savorelli et al. 2025) are unknown for the time being. Available data on the other phases figure a certain stability in the *Latonia*-dominated anuran assemblages, with a potential exception only at the beginning of phase 2 (Fig. 9C). However, see the "Results of the distribution analysis" section above for the caveats preventing a confident recognition of anuran distributional trends over the Gargano biostratigraphic phases at the moment, pending a clear assignment to a specific phase or subphase for most of the fissures with anuran fossils. A comprehensive framework for all the fissures should be a priority for future works on the Gargano Terre Rosse, to allow more precise faunal change analyses. An explanation for the observed stability in the Gargano anuran communities could be sought in the resilience and generalist ecology that can be inferred for the identified taxa, almost all of which have extant relatives inhabiting a wide array of environments (see

e.g. Lanza et al. 2007; Speybroeck et al. 2016; Perl et al. 2017; Di Nicola et al. 2019; Razzetti et al. 2025). Extant *Latonia* is limited to a small marshy valley in the Levant (Mendelssohn and Steinitz 1943; Biton et al. 2013, 2016; Perl et al. 2017), but there they are encountered in both terrestrial and aquatic environments (Perl et al. 2017). The dominance of *Latonia* in the Terre Rosse might also reflect a similar, constant availability of diversified water bodies and associated terrestrial habitats. Other anurans add to this and further testify to the occurrence of temporary water bodies and, at least occasionally, of areas with abundant vegetation, based on the occurrences of green toads and tree frogs respectively (Lanza et al. 2007; Speybroeck et al. 2016; Di Nicola et al. 2019; Razzetti et al. 2025). Another factor potentially explaining the relative stability of anuran palaeocommunities in the Gargano palaeoisland is the geographical isolation itself: isolated contexts mean a lower dispersal of new competitors, thus leading to lower selection pressure and ultimately to the maintenance of community structure.

Taxonomic uncertainty on the Gargano anurans, together with the mentioned absence of clear examples of the earlier colonizing palaeocommunity, hinder the potential proposal of arguments useful to disentangle the problem of the geographic origins of the Late Miocene Terre Rosse insular fauna. The Gargano *Latonia* is part of a clade including highly sculptured members of the genus (i.e. the *L. seyfriedi* species complex; Fig. 10), which was widespread in Europe during the Miocene. Occurrences are reported from the Early Miocene of Czech Republic, Germany, and Greece, the Middle Miocene of France, Germany, Hungary, Poland, Romania, Serbia, Slovakia, Spain, and Switzerland, and the Late Miocene of Austria, Hungary, Spain, and Ukraine (Meyer 1843; Młynarski 1976; Młynarski et al. 1982; Hodrová 1987; Roček 1994, 2013, 2019; Sanchiz 1998; Rage and Hossini 2000; Miklas 2002; Böhme 2003, 2010; Venczel 2004, 2007; Hír and Venczel 2005; Tempfer 2005; Venczel et al. 2005; Venczel and Ştiucă 2008; Venczel and Hír 2013, 2015; Đurić 2016; Georgalis et al. 2019; Syromyatnikova et al. 2019; Villa et al. 2019; Delfino and Georgalis 2022; Pazonyi et al. 2025). Interestingly, none of the few other Italian Miocene occurrences of *Latonia*, all Messinian in age (Colombero et al. 2017; Villa et al. 2021), provided remains diagnostic enough to either confirm or refute their belonging to the *L. seyfriedi* group. On the other hand, the only species recognized in the Apennine Peninsula to date, the Early Pleistocene *Latonia dimenticata* Sorbelli et al., 2025, belonged to a different clade (Sorbelli et al. 2025). The topology recovered by our phylogenetic analysis (Fig. 10), with the new occurrence in a polytomy with *L. seyfriedi* and *L. kolebabi*, and the mixed characters shown by the remains herein described further complicate pinpointing continental populations potentially related to the ancestors of the Gargano *Latonia*. One interesting information provided by the Terre Rosse remains is the strong development of the tectum supraorbitale and the high density of the sculpturing in the frontoparietals. In their discussion about evolutionary trends of cranial exostosis in *Latonia*, Sorbelli et al. (2025) pointed out how this became less dense, and the tectum comparatively reduced starting with Late Miocene occurrences of the genus, maybe in relation to climate cooling. The degree of exostosis in the Gargano *Latonia* is more in agreement with older, Middle Miocene populations. A Middle Miocene ancestry for this *Latonia* would agree with the suggestion by Savorelli et al. (2017), who assumed such an ancestry for the erinaceid *Deinogalerix* Freudenthal, 1972. However, it conflicts with the murid dominated faunas of the palaeoislands, as Muridae only entered western Eurasia in the Late Miocene. Van den Hoek Ostende (2018) indicated that under insular conditions, lineages show a decoupling of general trends and may even display reverse evolution. The *Latonia* population would have encountered in the palaeoisland a stable environment (something also suggested by the little to no modification of the anuran communities over time) less influenced by ongoing climate change and, thus, maintained a certain degree of exostosis coverage. If correct, this further implies a decoupling from the main general trend for the evolution of isolated populations of *Latonia* and further highlights the insular character of the Gargano species.

Like *Latonia*, the other Terre Rosse anurans also belong to clades with a wide distribution in the circum-Mediterranean during the Miocene (Sanchiz 1998; Böhme 2003; Rage and Roček 2003; Roček 2013). Therefore, the same caveats apply to them as well, when it comes to potentially tracing back their ancestry and potential populations or areas of origin. Other Miocene occurrences in Italy of the same clades are also limited to a few Messinian localities (Colombero et al. 2014, 2017; Villa et al. 2021), not providing clear evidence of direct relationships with the Gargano ones. Conversely, other herptiles from Gargano provided more significant information on this ground: as a matter of fact, crocodylians from Gargano and the related Scontrone palaeoisland were likely dispersers from North Africa (Kotsakis et al. 2004; Delfino et al. 2007; Delfino and Rossi 2013). However, these crocodylians were able to actively engage in and more easily survive transmarine dispersal in the Mediterranean Sea due to high saltwater tolerance (Leslie and Taplin 2001; Cramp et al. 2008, 2010; Campbell et al. 2010), thus having access to a colonization route probably less available to anurans. However, long-distance transmarine anuran dispersal is indeed possible (e.g. Vences et al. 2003; Measey et al. 2007; Bell et al. 2015a, 2015b; Glaw et al. 2019; Marin da Fonte et al. 2019), and Savorelli et al. (2025) suggested rafting rather than land bridges as the most likely mode of colonisation for the Terre Rosse amphibians. The Gargano giant tortoises, on the other hand, are part of a clade of Mediterranean insular tortoises, the phylogenetic relationships of which are still enigmatic (Valenti et al. 2022; Georgalis et al. 2025). Furthermore, they are currently the oldest known occurrence of this clade (Georgalis et al. 2025), with large testudinids from Scontrone being older but currently still indeterminate at genus rank (Georgalis and Delfino 2021).

Future clarification of their closest relatives might also help in better establishing where to pinpoint the origin of the Late Miocene Gargano palaeoherpetofauna.

Conclusions

The poorly investigated palaeoherpetofauna from the Gargano Terre Rosse fissures already gave evidence of its peculiar and significant nature, highlighting the Late Miocene Gargano palaeoisland as a potential stepping stone for northward dispersal (Delfino et al. 2007) or an incubator for insular evolution (Villa and Delfino 2019; Georgalis et al. 2025) for amphibians and reptiles. Now, the anuran record from the fissures adds to this and provides more evidence for insularization and potential endemicity of the Gargano herptiles. The anurofauna is poorly diverse and scarcely represented, with 528 fossils recovered from 62 fissures and representing four different taxa: *Latonia* gr. *seyfriedi*, *Hyla* gr. *arborea*, aff. *Bufotes* gr. *viridis*, and *Pelophylax* sp. All of these pertain to clades that are widely distributed in Europe during the Miocene, thus not allowing to propose colonization routes or hypothetical geographical origins for the *Mikrotia* fauna or at least its amphibian component. Nevertheless, the morphology of the remains, including significant character mixture, the occurrence of rare osteological features, and (for *Latonia*) the development of exostosis and frontoparietal features different from other Late Miocene congenerics, indicates that the recognized assemblages represent anuran communities already affected by evolution in an insular context. Earlier, less insularized stages of the Gargano amphibian palaeocommunities are currently unknown, but a preliminary analysis of the biostratigraphic distribution suggests that they stayed more or less stable across different phases of the Gargano Terre Rosse faunal complex, being almost constantly represented by a *Latonia*-dominated and highly-adaptable anurofauna surviving into the Mediterranean environment of the palaeoisland.

Acknowledgements

The authors thank all the staff at JURASSICA for the organization of the 2025 RCMNS Workshop and the editors of this volume for inviting us to participate in it. Natasja den Ouden is warmly thanked for granting access to the RGM collection. We also acknowledge Hugues-Alexandre Blain and Tomáš Přikryl for sharing relevant literature, Omar Cirilli for help with Past and discussions over our preliminary results, Arnau Bolet for help with the phylogeny, and the Willi Hennig Society for making TNT freely available. With their suggestions, Alfred Lemierre and Bettina Reichenbacher helped improve an earlier version of this contribution during the review process. Anuran silhouettes used for Figs 5–9 are from PhyloPic (https://www.phylopic.org/). This is publication number 392 of the Museo di Geologia e Paleontologia collections at the Università degli Studi di Torino. We would like to dedicate this paper to the memory of the late Matthijs Freudenthal, whose legacy lives on in every new study on the Gargano Neogene faunas.

References

Abbazzi L, Angelone C, Arca M, Barisone G, Bedetti C, Delfino M, Kotsakis T, Marcolini F, Palombo MR, Pavia M, Piras P, Rook L, Torre D, Tuveri C, Valli AMF, Wilkens B (2004) Plio-Pleistocene fossil vertebrates of Monte Tuttavista (Orosei, Eastern Sardinia, Italy), an overview. Rivista Italiana di Paleontologia e Stratigrafia 110: 681–706. https://doi.org/10.13130/2039-4942/5832

Alcover JA, Sanders E, Sanchiz B (1984) El registro fósil de los sapos parteros (Anura, Discoglossidae) de Baleares. In: Hemmer H, Alcover JA (Eds) Història biològica del ferreret. Editorial Moll, Ciutat de Mallorca, 109–121.

Bailon S (1999) Différenciation ostéologique des anoures (Amphibia, Anura) de France. In: Desse J, Desse-Berset N (Eds) Fiches d'ostéologie animale pour l'Archéologie, Série C: Varia. Centre de Recherches Archéologiques-CNRS, Valbonne, 1–38.

Bell RC, Drewes RC, Channing A, Gvoždík V, Kielgast J, Lötters S, Stuart BL, Zamudio KR (2015a) Overseas dispersal of *Hyperolius* reed frogs from Central Africa to the oceanic islands of São Tomé and Príncipe. Journal of Biogeography 42: 65–75. https://doi.org/10.1111/jbi.12412

Bell RC, Drewes RC, Zamudio KR (2015b) Reed frog diversification in the Gulf of Guinea: overseas dispersal, the progression rule, and *in situ* speciation. Evolution 69: 904–915. https://doi.org/10.1111/evo.12623

Birbele E, Di Marzio A, Grauda D, Vimercati G, Deksne G (2023) Genetic diversity of European tree frogs (*Hyla arborea* group): A systematic review. ARPHA Preprints 4: e108466. https://doi.org/10.3897/arphapreprints.e108466

Biton R, Geffen E, Vences M, Cohen O, Bailon S, Rabinovich R, Malka Y, Oron T, Boistel R, Brumfeld V, Gafny S (2013) The rediscovered Hula painted frog is a living fossil. Nature Communications 4: 1959. https://doi.org/10.1038/ncomms2959

Biton R, Boistel R, Rabinovich R, Gafny S, Brumfeld V, Bailon S (2016) Osteological observations on the alytid anura *Latonia nigriventer* with comments on functional morphology, biogeography, and evolutionary history. Journal of Morphology 277: 1131–1145. https://doi.org/10.1002/jmor.20562

Blain H-A, Gibert L, Ferràndez-Cañadell C (2010) First report of a green toad (*Bufo viridis* sensu lato) in the Early Pleistocene of Spain: palaeobiogeographical and palaeoecological implications. Comptes Rendus Palevol 9: 487–497. https://doi.org/10.1016/j.crpv.2010.10.002

Blain H-A, Lózano-Fernández I, Böhme G (2015) Variation in the ilium of central European water frogs *Pelophylax* (Amphibia, Ranidae) and its implications for species-level identification of fragmentary anuran fossils. Zoological Studies 54: 5. https://doi.org/10.1186/s40555-014-0094-3

Böhme M (2003) The Miocene Climatic Optimum: evidence from ectothermic vertebrates of Central Europe. Palaeogeography, Palaeoclimatology, Palaeoecology 195: 389–401. https://doi.org/10.1016/S0031-0182(03)00367-5

Böhme M (2010) Ectothermic vertebrates (Actinopterygii, Allocaudata, Urodela, Anura, Crocodylia, Squamata) from the Miocene of Sandelzhausen (Germany, Bavaria) and their implications for environment reconstruction and palaeoclimate. Paläontologische Zeitschrift 84: 3–41. https://doi.org/10.1007/s12542-010-0050-4

Campbell HA, Watts ME, Sullivan S, Read AM, Choukroun S, Irwin SR, Franklin CE (2010) Estuarine crocodiles ride surface currents to facilitate long-distance travel. Journal of Animal Ecology 79: 955–964. https://doi.org/10.1111/j.1365-2656.2010.01709.x

Cattaneo A, Cattaneo C, Grano M (2023) The herpetofauna of the Dodecanese Islands. In: Masseti M (Ed.) Life on islands. 2. Zoological diversity of the Aegean Archipelago. Studies dedicated to Norma Chapmann. Edizioni Danaus, Palermo, 37–58.

Cayuela H, Valenzuela-Sánchez A, Teulier L, Martínez-Solano Í, Léna J-P, Merilä J, Muths E, Shine R, Quay L, Denoël M, Clobert J, Schmidt BR (2020) Determinants and consequences of dispersal in vertebrates with complex life cycles: a review of pond-breeding amphibians. Quarterly Review of Biology 95: 1–36. https://doi.org/10.1086/707862

Cirilli O, Benvenuti MG, Carnevale G, Casanovas Vilar I, Delfino M, Furió M, Papini M, Villa A, Rook L (2016) Fosso della Fittaia: the oldest Tusco-Sardinian late Miocene endemic vertebrate assemblages (Baccinello-Cinigiano Basin, Tuscany, Italy). Rivista Italiana di Paleontologia e Stratigrafia 122: 13–34. https://doi.org/10.13130/2039-4942/7166

Colombero S, Angelone C, Bonelli E, Carnevale G, Cavallo O, Delfino M, Giuntelli P, Mazza P, Pavia G, Pavia M, Repetto G (2014) The upper Messinian assemblages of fossil vertebrate remains of Verduno (NW Italy): Another brick for a latest Miocene bridge across the Mediterranean. Neues Jahrbuch für Geologie und Paläontologie – Abhandlungen 272: 287–324. https://doi.org/10.1127/0077-7749/2014/0408

Colombero S, Alba DM, D'Amico C, Delfino M, Esu D, Giuntelli P, Harzhauser M, Mazza PPA, Mosca M, Neubauer TA, Pavia G, Pavia M, Villa A, Carnevale G (2017) Late Messinian mollusks and vertebrates from Moncucco Torinese, north-western Italy. Paleoecological and paleoclimatological implications. Palaeontologia Electronica 20.1.10A: 1–66. https://doi.org/10.26879/658

Cramp RL, Meyer EA, Sparks N, Franklin CE (2008) Functional and morphological plasticity of crocodile (*Crocodylus porosus*) salt glands. Journal of Experimental Biology 211: 1482–1489. https://doi.org/10.1242/jeb.015636

Cramp RL, Hudson NJ, Franklin CE (2010) Activity, abundance, distribution and expression of Na^+/K^+-ATPase in the salt glands of *Crocodylus porosus* following chronic saltwater acclimation. Journal of Experimental Biology 213: 1301–1308. https://doi.org/10.1242/jeb.039305

Delaugerre M, Cheylan M (1992) Atlas de repartition des batraciens et reptiles de Corse. L'Oikéma, Pamplona, 128 pp.

Delfino M (2002) Erpetofaune italiane del Neogene e del Quaternario. PhD Thesis, Università degli Studi di Modena e Reggio Emilia, Modena, Italy.

Delfino M, Georgalis GL (2022) The fossil record of amphibians (Amphibia: Urodela and Anura) in Greece. In: Vlachos E (Ed.) Fossil Vertebrates of Greece, Vol. 1. Springer, Cham, 185–203. https://doi.org/10.1007/978-3-030-68398-6_6

Delfino M, Rook L (2008) The fossil amphibians and reptiles of Sardinia: a summary. In: Corti C (Ed.) Herpetologia Sardiniae. Societas Herpetologica Italica/Edizioni Belvedere, Latina, 192–195.

Delfino M, Rossi MA (2013) Fossil crocodylid remains from Scontrone (Tortonian, Southern Italy) and the late Neogene Mediterranean biogeography of crocodylians. Geobios 46: 25–31. https://doi.org/10.1016/j.geobios.2012.10.006

Delfino M, Razzetti E, Salvidio S (2005) European plethodontids: palaeontological data and biogeographical considerations. Atti del Museo Civico di Storia Naturale "G. Doria" di Genova 97: 45–58.

Delfino M, Böhme M, Rook L (2007) First European evidence for transcontinental dispersal of *Crocodylus* (late Neogene of southern Italy). Zoological Journal of the Linnean Society 149: 293–307. https://doi.org/10.1111/j.1096-3642.2007.00248.x

Delfino M, Bailon S, Pitruzzella G (2011) The Late Pliocene amphibians and reptiles from "Capo Mannu D1 Local Fauna" (Mandriola, Sardinia, Italy). Geodiversitas 33: 357–382. https://doi.org/10.5252/g2011n2a10

Di Nicola MR, Cavigioli L, Luiselli L, Andreone F (2019) Anfibi & rettili d'Italia. Edizioni Belvedere, Latina, 568 pp.

Dubois A, Bour R (2010) The nomenclatural status of the nomina of amphibians and reptiles created by Garsault (1764), with a parsimonious solution to an old nomenclatural problem regarding the genus *Bufo* (Amphibia, Anura) and comments on some nomina created by Laurenti (1768). Zootaxa 2447: 1–52. https://doi.org/10.11646/zootaxa.2447.1.1

Đurić D (2016) The early Miocene herpetofauna (Amphibia and Squamata) from Sibnica, Serbia. In: Marković Z, Milivojević M (Eds) Life on the shore: Geological and paleontological research in the Neogene of Sibnica and vicinity (Levač basin, Central Serbia) – Part 1. Special issue of the Natural History Museum in Belgrade, 57–61.

Freudenthal M (1971) Neogene vertebrates from the Gargano Peninsula, Italy. Scripta Geologica 3: 1–10.

Freudenthal M (1976) Rodent stratigraphy of some Miocene fissure fillings in Gargano (prov. Foggia, Italy). Scripta Geologica 37: 1–23.

Freudenthal M, Martín-Suárez E (2010) The age of immigration of the vertebrate faunas found at Gargano (Apulia, Italy) and Scontrone (l'Aquila, Italy). Comptes Rendus Palevol 9: 95–100. https://doi.org/10.1016/j.crpv.2009.12.004

Freudenthal M, Van den Hoek Ostende LW, Martín-Suárez E (2013) When and how did the *Mikrotia* fauna reach Gargano (Apulia, Italy)? Geobios 46: 105–109. https://doi.org/10.1016/j.geobios.2012.10.004

Georgalis GL, Delfino M (2021) The Scontrone turtles – A new insular testudinoid fauna from the late Miocene of the Central Mediterranean. Geobios 68: 71–81. https://doi.org/10.1016/j.geobios.2021.05.001

Georgalis GL, Villa A, Vlachos E, Delfino M (2016) Fossil amphibians and reptiles from Plakias, Crete: a glimpse into the earliest late Miocene herpetofaunas of southeastern Europe. Geobios 49: 433–444. https://doi.org/10.1016/j.geobios.2016.09.004

Georgalis GL, Villa A, Ivanov M, Roussiakis S, Skandalos P, Delfino M (2019) Early Miocene herpetofaunas from the Greek localities of Aliveri and Karydia – bridging a gap in the knowledge of amphibians and reptiles from the early Neogene of southeastern Europe. Historical Biology 31: 1045–1064. https://doi.org/10.1080/08912963.2017.1417404

Georgalis GL, Vlachos E, Camanni F, Villa A, Pavia M, van den Hoek Ostende LW, Delfino M (2025) Testudinid turtle remains from the Late Miocene palaeo-island of Gargano, Italy, and an overview of Mediterranean insular tortoises. Swiss Journal of Palaeontology 144: 61. https://doi.org/10.1186/s13358-025-00402-4

Glaw F, Hawlitschek O, Glaw K, Vences M (2019) Integrative evidence confirms new endemic island frogs and transmarine dispersal of amphibians between Madagascar and Mayotte (Comoros archipelago). The Science of Nature 106: 19. https://doi.org/10.1007/s00114-019-1618-9

Gleed-Owen CP (1998) Quaternary herpetofaunas of the British Isles: Taxonomic descriptions, palaeoenvironmental reconstructions, and biostratigraphic implications. PhD Thesis, Coventry University, Coventry, United Kingdom.

Goloboff PA, Morales ME (2023) TNT version 1.6, with a graphical interface for MacOS and Linux, including new routines in parallel. Cladistics 39: 144–153. https://doi.org/10.1111/cla.12524

Gómez RO, Turazzini GF (2016) An overview of the ilium of anurans (Lissamphibia, Salientia), with a critical appraisal of the terminology and primary homology of main ilial features. Journal of Vertebrate Paleontology 36: e1030023. https://doi.org/10.1080/02724634.2015.1030023

Hammer Ø, Harper DAT, Ryan PD (2001) PAST: Paleontological statistics software package for education and data analysis. Palaeontologia Electronica 4: art. 4.

Hír J, Venczel M (2005) New Middle Miocene vertebrate localities from Subpiatră (Bihor district, Romania). Acta Palaeontologica Romaniae 5: 211–221.

Hodrová M (1987) Lower Miocene frogs from the Dolnice locality in the Cheb Basin (Czechoslovakia). Acta Universitas Carolinae - Geologica 2: 97–115.

Holman JA (1998) Pleistocene amphibians and reptiles in Britain and Europe. Oxford Monographs on Geology and Geophysics 38: 1–254. https://doi.org/10.1093/oso/9780195112320.001.0001

Hopkins GR, Brodie Jr ED (2015) Occurrence of amphibians in saline habitats: a review and evolutionary perspective. Herpetological Monographs 29: 1–27. https://doi.org/10.1655/HERPMONOGRAPHS-D-14-00006

Kotsakis T (1980) I resti di anfibi e rettili pleistocenici della grotta di Dragonara (Capo Caccia, Sardegna). Geologica Romana 19: 85–90.

Kotsakis T (1982) Presence du genre *Discoglossus* Otth (Discoglossidae, Anura, Amphibia) dans le Villafranchien de l'Ile de Crete. Geologica Romana 21: 185–189.

Kotsakis T, Delfino M, Piras P (2004) Italian Cenozoic crocodilians: taxa, timing and palaeobiogeographic implications. Palaeogeography, Palaeoclimatology, Palaeoecology 210: 67–87. https://doi.org/10.1016/j.palaeo.2004.03.013

Lanza B (1984) Sul significato biogeografico delle isole fossili, con particolare riferimento all'arcipelago pliocenico della Toscana. Atti della Società Italiana di Scienze Naturali e del Museo Civico di Storia Naturale di Milano 125: 145–158.

Lanza B, Andreone F, Bologna MA, Corti C, Razzetti E (2007) Fauna d'Italia. Vol. 42. Amphibia. Edagricole, Milano, 537 pp.

Lemierre A, Blackburn DC (2022) A new genus and species of frog from the Kem Kem (Morocco), the second neobatrachian from Cretaceous Africa. PeerJ 10: e13699. https://doi.org/10.7717/peerj.13699

Leslie AJ, Taplin LE (2001) Recent development in osmoregulation of crocodilians. In: Grigg GC, Seebacher F, Franklin CE (Eds) Crocodilian biology and evolution. Surrey Betty & Sons, Chipping Norton, 265–279.

Lourenço A, Sequeira F, Buckley D, Velo-Antón G (2018) Role of colonization history and species-specific traits on contemporary genetic variation of two salamander species in a Holocene island-mainland system. Journal of Biogeography 45: 1054–1066. https://doi.org/10.1111/jbi.13192

Macaluso L, Villa A, Pitruzzella G, Rook L, Carnevale G, Delfino M (2021) A progressive extirpation: an overview of the fossil record of *Salamandrina* (Salamandridae, Urodela). Historical Biology 33: 3723–3740. https://doi.org/10.1080/08912963.2021.1888946

Macaluso L, Mannion PD, Evans SE, Carnevale G, Monti S, Marchitelli D, Delfino M (2022) Biogeographic history of Palearctic caudates revealed by a critical appraisal of their fossil record quality and spatio-temporal distribution. Royal Society Open Science 9: 220935. https://doi.org/10.1098/rsos.220935

Maddison WP, Maddison DR (2025) Mesquite: A modular system for evolutionary analysis. Version 4.02. https://www.mesquiteproject.org

Marin da Fonte LF, Mayer M, Lötters S (2019) Long-distance dispersal in amphibians. Frontiers of Biogeography 11(4): e44577. https://doi.org/10.21425/F5FBG44577

Martín C, Alonso-Zarazaga MA, Sanchiz B (2012) Nomenclatural notes on living and fossil amphibians. Graellsia 68: 159–180. https://doi.org/10.3989/graellsia.2012.v68.056

Masini F, Rinaldi PM, Petruso D, Surdi G (2010) The Gargano Terre Rosse insular faunas: an overview. Rivista Italiana di Paleontologia e Stratigrafia 116: 421–435. https://doi.org/10.13130/2039-4942/6396

Masini F, Rinaldi PM, Savorelli A, Pavia M (2013) A new small mammal assemblage from the M013 Terre Rosse fissure filling (Gargano, South-Eastern Italy). Geobios 46: 49–61. https://doi.org/10.1016/j.geobios.2012.10.003

Mazza PPA, Rustioni M (2008) Processes of island colonization by Oligo-Miocene land mammals in the central Mediterranean: New data from Scontrone (Abruzzo, Central Italy) and Gargano (Apulia, Southern Italy). Palaeogeography, Palaeoclimatology, Palaeoecology 267: 208–215. https://doi.org/10.1016/j.palaeo.2008.06.018

Measey GJ, Vences M, Drewes RC, Chiari Y, Melo M, Bourles B (2007) Freshwater paths across the ocean: molecular phylogeny of the frog *Ptychadena newtoni* gives insights into amphibian colonization of oceanic islands. Journal of Biogeography 34: 7–20. https://doi.org/10.1111/j.1365-2699.2006.01589.x

Mendelssohn H, Steinitz H (1943) A new frog from Palestine. Copeia 1943(4): 231–233. https://doi.org/10.2307/1438135

Mettouris O, Kornilios P (2015) A first record of the smooth newt, *Lissotriton vulgaris* (Linnaeus, 1758), from Samothraki island, NE Aegean Sea, Greece. Herpetology Notes 8: 483–484.

Meyer H von (1843) Mittheilungen an Professor Bronn gerichtet. Neues Jahrbuch für Mineralogie, Geologie und Paläontologie 1843: 579–590.

Miklas PM (2002) Die Amphibienfauna (Amphibia: Caudata, Anura) der obermiozänen Fundstelle Götzendorf an der Leitha (südliches Wiener Becken, Niederösterreich). Annalen des Naturhistorischen Museums in Wien 103A: 161–211.

Młynarski M (1976) *Discoglossus giganteus* Wettstein-Westersheimb, 1955 (Discoglossidae, Anura) from the Miocene of Przeworno in Silesia (Poland). Acta Zoologica Cracoviensia 21: 1–12.

Młynarski M, Szyndlar Z, Estes R, Sanchíz B (1982) Lower vertebrate fauna from the Miocene of Opole (Poland). Estudios Geológicos 38: 103–119.

Moncunill-Solé B, Quintana Cardona J, Blanco A, Rothschild BM (2026) Skeletal and dental anomalies provide insights into insular vertebrate zoology and evolution in Plio-Holocene Menorca, Western Mediterranean. Current Zoology: zoag023. https://doi.org/10.1093/cz/zoag023

Pazonyi P, Mészáros L, Szentesi Z, Segesdi M, Horáček I, Maul LC, Hir J (2025) A new, extraordinarily diverse, earliest Late Miocene (early Turolian, MN 11) small vertebrate "reference" assemblage from the Csodabogyós Cave (Keszthely Hills, Western Hungary). Fossil Imprint 81: 114–153. https://doi.org/10.37520/fi.2025.009

Perl RGB, Gafny S, Malka Y, Renan S, Woodhams DC, Rollins-Smith L, Pask JD, Bletz MC, Geffen E, Vences M (2017) Natural history and conservation of the rediscovered Hula painted frog, *Latonia nigriventer*. Contributions to Zoology 86: 11–37. https://doi.org/10.1163/18759866-08601002

Quintana J, Alcover JA, Moyà-Solà S, Sanchiz B (2005) Presence of *Latonia* (Anura, Discoglossidae) in the insular Pliocene of Menorca (Balearic Islands). Monografies de la Societat d'Història Natural de les Balears 12: 293–296.

Rage J-C, Hossini S (2000) Les amphibiens du Miocène moyen de Sansan. Mémoires du Muséum national d'Histoire naturelle 183: 177–217.

Rage J-C, Roček Z (2003) Evolution of anuran assemblages in the Tertiary and Quaternary of Europe, in the context of palaeoclimate and palaeogeography. Amphibia-Reptilia 24: 133–167. https://doi.org/10.1163/156853803322390408

Ratnikov VYu (2001) Osteology of Russian toads and frogs for paleontological researches. Acta Zoologica Cracoviensia 44: 1–23.

Razzetti E, Bruni G, Di Tizio L, Liuzzi C, Sindaco R (2025) Atlante degli anfibi e dei rettili d'Italia/Atlas of Italian amphibians and reptiles. Societas Herpetologica Italica/Edizioni Belvedere, Latina, 560 pp.

Rebouças R, da Silva HR, Solé M (2019) Malformations in insular and coastal populations of toads in Rio de Janeiro, Southeastern Brazil. South American Journal of Herpetology 14: 12–18. https://doi.org/10.2994/SAJH-D-17-00031.1

Reyes-Moya I, Sánchez-Montes G, Martínez-Solano Í (2022) Integrating dispersal, breeding and abundance data with graph theory for the characterization and management of functional connectivity in amphibian pondscapes. Landscape Ecology 37: 3159–3177. https://doi.org/10.1007/s10980-022-01520-x

Roček Z (1994) Taxonomy and distribution of tertiary discoglossids (Anura) of the genus *Latonia* v. Meyer, 1843. Geobios 27: 717–751. https://doi.org/10.1016/S0016-6995(94)80058-8

Roček Z (2013) Mesozoic and Tertiary Anura of Laurasia. Palaeobiodiversity and Palaeoenvironments 93: 397–439. https://doi.org/10.1007/s12549-013-0131-y

Roček Z (2019) A contribution to the herpetofauna from the late Miocene of Gritsev (Ukraine). Comptes Rendus Palevol 18: 817–847. https://doi.org/10.1016/j.crpv.2019.07.003

Rook L, Gallai G, Torre D (2006) Lands and endemic mammals in the Late Miocene of Italy: Constrains for paleogeographic outlines of Tyrrhenian area. Palaeogeography, Palaeoclimatology, Palaeoecology 238: 263–269. https://doi.org/10.1016/j.palaeo.2006.03.027

Sanchiz B (1981) Registro fosil y antiguedad de la familia Hylidae (Amphibia, Anura) en Europa. Anais, II Congreso Latino-americano de Paleontología 2: 757–764.

Sanchiz B (1998) Handbuch der Paläoherpetologie. 4 – Salientia. Friedrich Pfeil, München, 275 pp.

Sanchiz B, Mlynarski M (1979) Pliocene salamandrids (Amphibia, Caudata) from Poland. Acta Zoologica Cracoviensia 24: 175–188.

Sanchiz B, Sanz JL (1980) Los anfibios del Pleistoceno medio de Aridos-1 (Arganda, Madrid). In: Santonja M, López Martínez N, Pérez-González A (Eds) Ocupaciones achelenses en el valle del Jarama. Diputacion Provincial de Madrid, Madrid, 105–126.

Sanchiz FB (1977) La familia Bufonidae (Amphibia, Anura) en el Terciario europeo. Trabajos Neógeno-Cuaternario 8: 75–111.

Savona Ventura C (1984) The fossil herpetofauna of the Maltese islands, a review. Naturalista Siciliano 8: 93–106.

Savorelli A, Masini F (2016) *Mystemys giganteus* n. gen. et sp.: an enigmatic and rare cricetid from the Terre Rosse M013 fissure filling (Gargano, southeastern Italy). Palaeontographica Abteilung A 306: 1–23. https://doi.org/10.1127/pala/306/2016/1

Savorelli A, Colombero S, Masini F (2016) *Apatodemus degiulii* n. gen. et sp. (Rodentia, Muridae), a hitherto undescribed endemite from the Terre Rosse of Gargano (Late Miocene, Southeastern Italy). Palaeontographica Abteilung A 306: 25–49. https://doi.org/10.1127/pala/306/2016/25

Savorelli A, Masini F, Mazza PPA, Rossi MA, Agostini S (2017) New species of *Deinogalerix* (Mammalia, Eulipotyphla) from the late Miocene of Scontrone (Abruzzo, central Italy). Palaeontologia Electronica 20.1.16A: 1–26. https://doi.org/10.26879/672

Savorelli A, Mazza PPA, Borrani A, Delfino M, Pavia M, Masini F (2025) The palaeontological legacy of the Late Miocene Gargano's Terre Rosse (southeastern Italy): evolutionary patterns, adaptive radiations, and unresolved origins. Bollettino della Società Paleontologica Italiana 64: 313–335. https://doi.org/10.4435/BSPI.2025.16

Sigovini M, Keppel E, Tagliapietra D (2016) Open nomenclature in the biodiversity era. Methods in Ecology and Evolution 7: 1217–1225. https://doi.org/10.1111/2041-210X.12594

Sillero N, Campos J, Bonardi A, Corti C, Creemers R, Crochet P-A, Crnobrnja Isailović J, Denoël M, Ficetola GF, Gonçalves J, Kuzmin S, Lymberakis P, de Pous P, Rodríguez A, Sindaco R, Speybroeck J, Toxopeus B, Vieites DR, Vences M (2014) Updated distribution and biogeography of amphibians and reptiles of Europe. Amphibia-Reptilia 35: 1–31. https://doi.org/10.1163/15685381-00002935

Smith MA, Green DM (2005) Dispersal and the metapopulation paradigm in amphibian ecology and conservation: are all amphibian populations metapopulations? Ecography 28: 110–128. https://doi.org/10.1111/j.0906-7590.2005.04042.x

Sorbelli L, Azzarà B, Cherin M, Delfino M, Roček Z, Villa A (2025) Why extant, why not extinct? A new extinct *Latonia* species (Anura: Discoglossidae) from the Early Pleistocene of the Apennine Peninsula provides clues on the survival of the genus in Eurasia. Journal of Systematic Palaeontology 23: 2554727. https://doi.org/10.1080/14772019.2025.2554727

Speybroeck J, Beukema W, Bok B, Van der Voort J (2016) Field guide to the amphibians and reptiles of Britain and Europe. Bloomsbury Publishing, London, 432 pp.

Speybroeck J, Beukema W, Dufresnes C, Fritz U, Jablonski D, Lymberakis P, Martínez-Solano I, Razzetti E, Vamberger M, Vences M, Vörös J, Crochet P-A (2020) Species list of the European herpetofauna – 2020 update by the Taxonomic Committee of the Societas Europaea Herpetologica. Amphibia-Reptilia 41: 139–189. https://doi.org/10.1163/15685381-bja10010

Špinar Z, Klembara J, Meszároš Š (1993) A new toad from the Miocene at Devínska Nová Ves (Slovakia). Západné Karpaty, séria Paleontológia 17: 135–160.

Špinar ZV (1972) Tertiary frogs from Central Europe. Academia, Prague, 286 pp. https://doi.org/10.1007/978-94-010-2932-2

Syromyatnikova E, Roček Z (2019) New *Latonia* (Amphibia: Alytidae) from the late Miocene of northern Caucasus (Russia). Palaeobiodiversity and Palaeoenvironments 99: 495–509. https://doi.org/10.1007/s12549-018-0350-3

Syromyatnikova E, Roček Z, van de Velde S (2019) New discoveries in the frog *Latonia seyfriedi* (Anura: Alytidae) and their impact on taxonomy of the genus *Latonia*. PalZ 93: 669–677. https://doi.org/10.1007/s12542-019-00477-8

Syromyatnikova EV (2015) A new species of *Bufo* (Amphibia, Anura) from the Miocene of Russia. Russian Journal of Herpetology 22: 281–288.

Tempfer PM (2005) The herpetofauna (Amphibia: Caudata, Anura; Reptilia: Scleroglossa) of the Upper Miocene locality Kohfidisch (Burgenland, Austria). Beiträge zur Paläontologie 29: 145–253.

Tok CV, Çiçek K (2014) Amphibians and reptiles in the Province of Çanakkale (Marmara Region, Turkey). Herpetozoa 27: 65–76.

Torfstein A, Steinberg J (2020) The Oligo–Miocene closure of the Tethys Ocean and evolution of the proto-Mediterranean Sea. Scientific Reports 10: 13817. https://doi.org/10.1038/s41598-020-70652-4

Torres-Roig E, Bailon S, Bover P, Alcover JA (2017) An early Pliocene anuran assemblage from Mallorca (Balearic Islands, Western Mediterranean): palaeobiogeographic and palaeoenvironmental implications. Palaeobiodiversity and Palaeoenvironments 97: 315–327. https://doi.org/10.1007/s12549-017-0273-4

Valakos ED, Pafilis P, Sotiropoulos K, Lymberakis P, Maragou P, Foufopoulos J (2008) The amphibians and reptiles of Greece. Chimaira, Frankfurt am Main, 463 pp.

Valenti P, Vlachos E, Kehlmaier C, Fritz U, Georgalis GL, Luján ÀH, Miccichè R, Sineo L, Delfino M (2022) The last of the large-sized tortoises of the Mediterranean islands. Zoological Journal of the Linnean Society 196: 1704–1717. https://doi.org/10.1093/zoolinnean/zlac044

Van den Hoek Ostende LW (2018) Cladistics and insular evolution, an unfortunate marriage? Another tangle in the *Deinogalerix* analysis of Borrani et al. (2017). Cladistics 34: 708–713. https://doi.org/10.1111/cla.12238

Van den Hoek Ostende LW, Meijer HJM, van der Geer AAE (2009) A bridge too far. Comment on "Processes of island colonization by Oligo-Miocene land mammals in the central Mediterranean: New data from Scontrone (Abruzzo, Central Italy) and Gargano (Apulia, Southern Italy)" by P.P.A. Mazza and M. Rustioni [Palaeogeography, Palaeoclimatology, Palaeoecology 267 (2008) 208–215]. Palaeogeography, Palaeoclimatology, Palaeoecology 279: 128–130. https://doi.org/10.1016/j.palaeo.2009.02.029

Vasileiadou K, Böhme M, Neubauer TA, Georgalis GL, Syrides GE, Papadopoulou L, Zouros N (2017) Early Miocene gastropod and ectothermic vertebrate remains from the Lesvos Petrified Forest (Greece). PalZ 91: 541–564. https://doi.org/10.1007/s12542-017-0352-x

Vences M, Vieites DR, Glaw F, Brinkmann H, Kosuch J, Veith M, Meyer A (2003) Multiple overseas dispersal in amphibians. Proceedings of the Royal Society of London. Series B: Biological Sciences 270: 2435–2442. https://doi.org/10.1098/rspb.2003.2516

Venczel M (2004) Middle Miocene anurans from the Carpathian Basin. Palaeontographica Abteilung A 271: 151–174. https://doi.org/10.1127/pala/271/2004/151

Venczel M (2007) Late Middle Miocene amphibians and reptiles from Subpiatrâ (Bihor district, Romania). Nymphaea, Folia Naturae Bihariae 34: 39–66.

Venczel M, Hír J (2013) Amphibians and squamates from the Miocene of Felsötárkány Basin, N-Hungary. Palaeontographica Abteilung A 300: 117–158. https://doi.org/10.1127/pala/300/2013/117

Venczel M, Hír J (2015) Lissamphibians and squamate reptiles from the early middle Miocene of Litke, Northern Hungary. Geobios 48: 491–504. https://doi.org/10.1016/j.geobios.2015.09.001

Venczel M, Sanchíz B (2006) Lower Miocene amphibians and reptiles from Oschiri (Sardinia, Italy). Hantkeniana 5: 72–75.

Venczel M, Ştiucă E (2008) Late middle Miocene amphibians and squamate reptiles from Tauţ, Romania. Geodiversitas 30: 731–763.

Venczel M, Hír J, Huza RR, Popa E, Golban D (2005) A new Middle Miocene vertebrate fauna from Subpiatră (Bihor County, Romania). Nymphaea, Folia Naturae Bihariae 32: 23–38.

Vigne J-D, Bailon S, Cuisin J (1997) Biostratigraphy of amphibians, reptiles, birds and mammals in Corsica and the role of man in the Holocene faunal turnover. Anthropozoologica 25/26: 587–604.

Villa A, Delfino M (2019) Fossil lizards and worm lizards (Reptilia, Squamata) from the Neogene and Quaternary of Europe: an overview. Swiss Journal of Palaeontology 138: 177–211. https://doi.org/10.1007/s13358-018-0172-y

Villa A, Roček Z, Tschopp E, van den Hoek Ostende LW, Delfino M (2016) *Palaeobatrachus eurydices*, sp. nov. (Amphibia, Anura), the last western European palaeobatrachid. Journal of Vertebrate Paleontology 36: e1211664. https://doi.org/10.1080/02724634.2016.1211664

Villa A, Delfino M, Luján ÀH, Almécija S, Alba DM (2019) First record of *Latonia gigantea* (Anura, Alytidae) from the Iberian Peninsula. Historical Biology 31: 371–382. https://doi.org/10.1080/08912963.2017.1371712

Villa A, Bacciotti M, Sala B, Delfino M (2020) Early Biharian amphibians and reptiles from Monte La Mesa (Verona, northeastern Italy): a typical herpetological assemblage from the Early Pleistocene of Veneto. Bollettino della Società Paleontologica Italiana 59: 85–104. https://doi.org/10.4435/BSPI.2020.01

Villa A, Carnevale G, Pavia M, Rook L, Sami M, Szyndlar Z, Delfino M (2021) An overview of the late Miocene vertebrates from the fissure fillings of Monticino Quarry (Brisighella, Italy), with new data on non-mammalian taxa. Rivista Italiana di Paleontologia e Stratigrafia 127: 297–354. https://doi.org/10.13130/2039-4942/15774

Zotos S, Stamatious M, Vogiatzakis IN (2023) The Cyprus Herp Atlas: An initiative for systematic recording of amphibian and reptile occurrences in Cyprus. Biodiversity Data Journal 11: e98142. https://doi.org/10.3897/BDJ.11.e98142

Additional information

Conflict of interest

The authors have declared that no competing interests exist.

Ethical statement

No ethical statement was reported.

Artificial Intelligence (AI) use

The authors accept full responsibility for the content of the manuscript, including the disclosure of any use of AI.
No AI tools were used in the preparation of this manuscript.

Funding

Research supported by: Agencia Estatal de Investigación, Spanish Ministerio de Ciencia e Innovación (MICIU/AEI/10.13039/501100011033) and FSE+ (PID2024-159434NB-I00; RYC2024-048550-I); Secretaria d'Universitats i Recerca of the Departament de Recerca i Universitats, Generalitat de Catalunya (2021 BP 00038), CERCA Programme/Generalitat de Catalunya; SYNTHESYS 4 programme fellowship (MP), RILO 2018-2024, GIF 2025 (MD, MP).

Author contributions

Conceptualization, Methodology, Validation, Supervision, Project administration: AV, MP, MD; Formal analysis: AV, MD; Investigation: AV, MD; Data Curation: MP, LR, LWHO, MD; Writing - Original draft: AV, DM; Writing - Review and Editing: all authors; Visualization: AV, DM; Funding Acquisition: AV, MP, MD.

Author ORCIDs

A. Villa https://orcid.org/0000-0001-6544-5201
D. Marchitelli https://orcid.org/0009-0006-4261-5881
M. Pavia https://orcid.org/0000-0002-5188-4155
L. Rook https://orcid.org/0000-0001-8923-5428
L.W. van den Hoek Ostende https://orcid.org/0000-0003-3114-0121
M. Delfino https://orcid.org/0000-0001-7836-7265

Data availability

All the fossils studied for this work are housed in public collections (see Material and methods). All data are provided within the article text or as part of the supplementary materials.

Supplementary material 1

Complete list of the fossils studied for this work and distribution of identified taxa per fissure

Authors: Andrea Villa, Domenico Marchitelli, Marco Pavia, Lorenzo Rook, Lars W. van den Hoek Ostende, Massimo Delfino
Data type: xlsx
Explanation note: Detailed information is provided with respect to hosting collection, repository number, fissure of provenance, taxon, skeletal element, quantity of elements per repository number, and siding of the elements. Distribution is calculated as minimum number of individuals (MNI) and number of identifiable specimens (NISP). Note that, for Anura indet., MNI indicates the presence of an additional individual compared with those estimated for other taxa in the same fissure: e.g. if a fissure yielded three right ilia of *Latonia* gr. *seyfriedi*, leading to a MNI = 3, one right ilium of *Hyla* gr. *arborea* (MNI = 1), and one right and four left ilia identified as Anura indet., the reported MNI for the latter taxon is 1, because only one ilium (the right one) could not represent the unidentifiable missing ilium for the individuals of the other taxa.
Copyright notice: This dataset is made available under the Open Database License (http://opendatacommons.org/licenses/odbl/1.0). The Open Database License (ODbL) is a license agreement intended to allow users to freely share, modify, and use this Dataset while maintaining this same freedom for others, provided that the original source and author(s) are credited.
Link: https://doi.org/10.3897/sjp.145.206406.suppl1

Supplementary material 2

Phylogenetic matrix used to conduct the phylogenetic analysis, based on the original matrix by Sorbelli et al. (2025)

Authors: Andrea Villa, Domenico Marchitelli, Marco Pavia, Lorenzo Rook, Lars W. van den Hoek Ostende, Massimo Delfino
Data type: nex
Copyright notice: This dataset is made available under the Open Database License (http://opendatacommons.org/licenses/odbl/1.0). The Open Database License (ODbL) is a license agreement intended to allow users to freely share, modify, and use this Dataset while maintaining this same freedom for others, provided that the original source and author(s) are credited.
Link: https://doi.org/10.3897/sjp.145.206406.suppl2